Perfusion Bioreactor System for Real Time Metabolic Profiling of 3D Human Adipose Tissue

A thesis

submitted by

Andrew D. Ward

In partial fulfillment of the requirements

for the degree of

Masters of Science

In

Biomedical Engineering

TUFTS UNIVERSITY

February 2012

Adviser: David Kaplan, PhD

Committee member: Professor Irene Georgakoudi, PhD

Cross department committee member: Professor Gary Leisk, PhD

Abstract

The aim of this research has been to develop and test a novel bioreactor system compatible with advanced multi photon imaging modalities for redox ratio analysis and media extraction capabilities for the purpose of improving the methods by which human biological samples are studied. The physiological relevance of the tissue environment was improved by designing in perfusion capabilities and using 3D human vascularized adipose tissue constructs. The analytical techniques used were an improvement from the industry standards of destructive histological stains and lysed cell assays. Noninvasive real time analysis of the morphology and metabolism of the adipose tissue was implemented through two photon excited fluorescence imaging. Depth resolved images ranging from 0-200 μm depths were taken to acquire a 3D representation of the tissue morphology. These image stacks were then further analyzed for subsequent redox ratio analysis, and the data acquired in this system was compared with data acquired in experiments previously conducted in another lab where a similar analysis was performed on 3D engineered adipose tissue in static culture. The experiments conducted here in perfusion culture yielded different results than those performed in static culture with regard to intra tissue cellular localization and redox ratio calculations. However, the overall trend of decreased redox ratios and cellular proliferation were similar across both static and perfusion culture.

Acknowledgments

I would like to thank my advisor, Professor David Kaplan, for his role in guiding me throughout the entirety of my Masters of Science experience, but most importantly for instilling in me an interest in Biomedical Engineering as a professor and mentor starting from my undergraduate career through to today.

I would also like to thank the great support I received throughout the rest of the Tufts Biomedical Engineering Department throughout my research from the graduate students and other researchers. I owe my involvement in Biomedical Engineering to the direction and mentorship of Jonathan Kluge and Michael House.

As a graduate student, I owe the most thanks to Evangelia Bellas, who has taught me everything from basic cell culture to tissue engineering and staining. She has played an integral and invaluable role in just about every aspect of my thesis. I would also like to thank Kyle Quinn for his continued efforts in training and looking over all my imaging work and subsequent redox ratio analysis and interpretation.

Lastly, I wish to express my sincere appreciation for the Soft Tissue Disease Models group and the entire Kaplan Lab and staff. It was only through their unfailing support and guidance that I was able to be successful in any aspect of my research.

Table of Contents

List of Tables

List of Figures

INTRODUCTION

There exists a need for improved methods of understanding and characterizing the metabolic activity of relevant biological specimens within appropriate *in vitro* environments. The metabolism of a biological system dictates the flow of energy and direction of energy within that system. This is energy flow, or metabolic behavior, is dependent on both intracellular and extracellular signaling. Understanding what a particular population of cells is using its energy for and where it is obtaining this energy from provides insight into the priorities of a cell's function at a particular instant. Cellular differentiation, proliferation, growth, anabolism, and drug response are all factors that affect the metabolic state of a cell/tissue system. Understanding these factors is paramount in elucidating clinical treatments for injuries, pathogenesis, and toxicity. Current analytical tools used to measure these traits are often destructive analysis that provide information only to the one metabolic/morphological activity of the tissue at one time point, and provide no dynamic information on the flow of energy throughout any particular tissue at different time points. This is why it is important to devise an improved system with capabilities of monitoring metabolic activity to study in real time the metabolic behavior of biological tissues with human clinical relevance.

With respect to drug screening, there are currently many methods used to predict the effects of drugs on humans prior to clinical trials. The most common include 2D cell assays in tissue culture plates and animal testing (Paul et al., 2010; Kola and Landis, 2010). More recently, engineered 3D tissues have become a mode by which human metabolism and tissue morphology can be studied as a function of maturity, drug delivery, and pathogenesis (MP Research Labs, Spinnerstown, PA; Zghoul et al., 2010).

Each of these techniques has their own strengths and limitations, as shown in Table 1. 2D tissue culture plate systems lack the ability to emulate 3D extracellular matrix-cell signaling. Animal tests can be appropriate for some applications, but it is clear that for more complex treatments they fail to adequately represent how clinical treatments will affect humans. Current efforts that base their research off of 2D cell culture models and animal tests have lost efficacy, and these systems are in question throughout pharmaceutical and research industries (Kola and Landis, 2010).

Method	Strengths	Weaknesses
2D Cell Assays	- isolate the effects of a single drug on a particular cell type	-No 3D ECM structure to mimic complex mechanical/biochemical environments
Animal Testing	-Provides observation of the complex metabolic effects a drug has on an entire body -Helps mimic drug delivery (timed release effects)	-Drug effects may be different across species (human vs. animal) -Ethical issues -Difficulties in discerning how animal 'feels' in response to drugs
3D Tissues	-Some human 3D tissue systems reflect native human tissues -Allow for 3D ECM-cell signaling	-Destructive analysis -Not sustainable for weeks or months

Table 1. Comparison of the strengths and weakness of multiple commonly used drug screening methods.

For the more recently studied 3D human tissue systems, longevity of tissue viability and the burden of destructive analysis techniques limit the quality and efficiency of the research. Two such commercially available tissue systems are epidermal and respiratory

tract tissues (MatTek, Ashland, MA) made from normal human epidermal keratinocytes and normal human bronchial epithelial cells, respectively. Each of these tissues have been validated as appropriate human tissue models via lipid accumulation, electrical resistance, and microscopy, but have only been analyzed through destructive methods (i.e., histology) in order to observe changes in morphology/metabolism, and have only been shown capable of remaining viable for 3-4 weeks at best (Kola and Landis, 2010). Therefore, alternative approaches for metabolic monitoring and pharmaceutical/research optimization are needed prior to human clinical trials.

2D CULTURE AND CURRENT LIMITATIONS

Preliminary studies on any particular cell line or tissue begin with 2D cell culture analysis on tissue culture plastic. For clinical relevance, researchers focus these studies on human cell lines of the dominant cell type within a particular environment (i.e., adipocytes for adipose tissue studies, cardiomyocytes for heart tissue studies, etc.). From here, the metabolic effects of any particular treatment can be studied through biochemical assays and imaging. Any observed changes (protein expression, cell viability/proliferation/ differentiation) can be isolated to the cell line(s) being studied. However, this approach does not simulate the complex metabolic processes that would characterize the pharmacodynamic and pharmacokinetic effects that would characterize drug-tissue interactions in pharmaceutical research. Any research conducted using 2D tissue cultures using a select one or few cell lines fails to replicate the in vivo environment where a treatment is subjected to a multitude of cell types, enzymes, mechanical influences, immune response, and ECM-mediated interactions. For example, complications in drug

absorption, distribution, metabolism, and secretion when tested *in vivo* account for 39% of the attrition of drugs tested (Tingle and Helsby, 2005). Drug interactions with unexpected and unwanted organs/cells of the body lead to unacceptable toxicity levels in 21% of new drugs (Tingle and Helsby, 2005). These failure rates suggest a need for new modes to evaluate the metabolic effects of clinical treatments in more realistic human tissues.

ANIMAL MODELS AND CURRENT LIMITATIONS

Unlike cell assays conducted in *in vitro* settings, clinical treatments examined in animal models provide a more appropriate representation for how a treatment may react in complex metabolic environments *in vivo*. However, any treatment's effects can vary significantly across different animal species (Boucher et al., 1980). The anatomic differences across different species lead to differences in development, pathology vulnerability, physiology, metabolism, etc. These differences are evident in that different animals tend to be preferentially used to study different diseases. Felines have an affinity towards acquiring the immunodeficiency virus (FIV); armadillos are prone to leprosy, while dogs are the primary animal used to model the effects of narcolepsy (Dunham 2006; Job 2003). Despite the realistic and metabolically complex environment of testing drugs *in vivo* using animal models, they are still not accurate representations of the human *in vivo* environment when attempting to predict the effects of drugs intended for human applications.

TISSUE ENGINEERED SYSTEMS AND CURRRENT LIMITATIONS

3D tissue models have been developed and used for the purpose of studying the effects of drugs, UV radiation, cosmetics, topical applications and related treatments to engineered 3D human tissues (MB Research Labs, Spinnerstown, PA). MatTek (Ashland, MA) has engineered a protocol for 3D tracheal, corneal, gingival, buccal, vaginal, and epidermal human tissues. Many of their models have been validated as appropriate *in vitro* models for native tissues by exhibiting the necessary physical and biochemical properties that characterize their native counterparts (Netzlaff et al., 2005). In particular, the epidermal tissues from MatTek (Epiderm) and SkinEthic Labs (Episkin, Lyon, France) are considered suitable tissue models based on their observed morphological cues (measured via spectroscopy and histology), biochemical markers and lipid composition (Netzlaff et al., 2005). These criteria for assessing the adequacy of tissue engineered constructs for modeling native tissue have been accepted in the literature, and have motivated *in vitro* studies on the effects of drug delivery to human skin tissue (Zghoul et al., 2010).

The previously described tissue system Epiderm has been successfully used as a model to study the effects of prednicarbate (a commercially available drug) when applied in different preparations (ointment, cream) to human skin (Lombardi-Borgia et al., 2007). The data found from testing prednicarbate on Epiderm showed percutaneous absorption rates and esterase activity consistent with what would have been expected from testing on actual human skin.

However, in all of the 3D tissue models described, analysis for biochemical or morphological changes has required the sacrifice of the tissue. None of the above studies

have been conducted to allow continuous monitoring via imaging or media sampling to assess function of the tissues. Furthermore, some of the systems, including the epidermal model, have serious drawbacks in terms of sustainability of function due to loss of viability of cells over time or contamination (Poumay et al., 2006). These issues make it difficult to assess long term or chronic effects of drugs in vitro.

NONINVASIVE TISSUE ANALYSIS

Different optical imaging methods including confocal microscopy, fluorescence lifetime imaging, electron paramagnetic resonance imaging, and multi-photon fluorescence imaging can be used to analyze morphological and biochemical features of tissues (Provenzano et al., 2008; Rice et al., 2007; Spasojevic et al., 2011). It has been shown in previous experiments that metabolic activity and differentiation status can be assessed in human mesenchymal stem cells subjected to osteogenic or adipogenic differentiation medium by use of two photon excited fluorescence imaging (Rice et al., 2007; Rice et al., 2010). Metabolic activity can be a sign of a wide range of tissue functions including but not limited to tissue genesis, pathology, immune response, differentiation, and cell division. By utilizing noninvasive imaging methods, insight could be gained into the reaction of engineered tissues on a cellular level in response to different clinical treatments and/or tissue growth. Thus, the implication of these results is that 3D human tissues can be assessed in a nondestructive, real time, continuous fashion

SIGNIFICANCE

The importance of engineering a more efficient and effective method for testing drugs prior to human trials can be easily understood by analyzing the current state of the pharmaceutical industry. The price per earnings ratio (P/E) is a metric often used as a general assessment of an industry's financial viability and profitability. It represents the relative price of a company's stock divided by the annual earnings per share, and provides insight into how competitively sought after the stock is (a higher P/E implies a more competitive market). At present, the pharmaceutical industry's price per earnings ratio has decreased below that of the S&P 500 Index and has remained below this ratio for the past 7yrs (Congressional Budget Office). The reasons for the drop in the price per earnings ratio is mathematically described as a relative decrease in revenues for the industry compared to its costs. A cause of this is the fact that many drug patents held by large pharmaceutical companies have been expiring over the past 10yrs, and will continue to do so in the upcoming years as well. This leads to competition between the large pharmaceutical companies who develop these drugs, and smaller generic brands that are able to take over part of the market (Kola and Landis, 2010). The problem with this scenario is that the revenue lost from the companies who develop these drugs doesn't necessarily go into the research and development of new drugs. Instead, the generic firms take this money as pure profit, or to fund other sectors of their businesses causing a disincentive for large drug developing companies to continue in their research. The only solution to this dilemma would be to extend the length of time that drug patents can be held before generic drug firms can copy the drugs and market them, or to increase the

productivity and decrease the costs of the research and development sectors of the pharmaceutical industry.

Estimates made in March of 2010 indicate that each novel drug entity that is launched comes at a cost of $1.8billion to the pharmaceutical companies in R&D alone (Congressional Budget Office). This is a result of the overwhelming failure rates of newly developed drugs during clinical testing, and the large amount of time that is spent developing these drugs. At present, only 8% of novel therapeutic molecular entities adopted at the preclinical stages of drug development ever make it to launch, and each new launch only comes after an average of 13.5yrs of research, testing, and regulatory reviews for new drugs(Congressional Budget Office). This drastic attrition rate and lengthy timeline begs for a new procedure for testing the quality and toxicological effects of new drug molecular entities earlier in the drug discovery process. A solution to this problem can be found in the advances made in the biomedical sciences.

Large pharmaceutical companies are in need of a way to improve the efficiency of their R&D departments by both increasing the output of FDA approved drugs and decreasing the costs of development. If a novel method for improving efficiency of the current drug development process could be engineered in such a way that it would decrease the time and money required to develop drugs by improving the methods by which drugs are tested during preclinical stages, then these large companies would be able to remain competitive in the drug market in spite of the competition coming from generic drug companies, providing more incentives to the larger drug developing companies to continue their research and development into discovering new and helpful drugs.

NOVELTY AND INNOVATION

The combination of a perfusion bioreactor, long term sustainable adipose tissue, with nondestructive metabolic, biochemical, and morphological analysis makes this system innovative. Each of the components has been previously demonstrated in part by us as well as others; however, integration into a real time metabolic monitoring platform with perfusion and media sampling capabilities has not been accomplished previously. This type of system will provide a new option for real time metabolic monitoring as an attempt to improve current practices in the arenas of pharmaceutical drug discovery and biological research by providing the following capabilities:

- The ability to noninvasively monitor cell metabolism, as well as cell-matrix structure and function
- Screening of both short (acute) and long term (chronic) drug therapies.
- Monitoring different types of engineered or excised tissues.
- Integrate complex multiple tissue systems to metabolically profile in a dynamic, real time setting.

The ability to generate functional complex human tissues in a 3D format provides a new generation of options towards drug screening and *in vitro* biological research. As described earlier, this is innovative in that both noninvasive imagining and sustainability over long time frames can be integrated into one system. The ability to generate functional human tissues that can be grown from weeks to months is also a new direction in the field. With the scaffold designs and systems planned, we have shown that

functional tissues can be maintained for weeks to months and the goal is to expand on this feature. By integrating optical imaging interfaces to the system, real time continuous monitoring is permitted, offering the capability to noninvasively assess cell and tissue responses to growth and clinical treatments. Observations include but are not limited to metabolic activity, fat depot resorption, and ECM remodeling, offering a multifaceted approach to gather insight into multiple modes of drug impact on the cells and tissues using one system.

Little work has been done to test the effects of new drugs and topical applications on engineered human tissue *in vitro* outside of the cosmetics industry (and what has been done is constrained to mostly epidermal tissue) (Netzlaff et al., 2005). As mentioned earlier, the primary methods for testing new drugs are cell assays in static systems (e.g., usually tissue culture plates), and animal testing in rodents. Further, human white adipose tissue has not been extensively studied as a model for testing the effects of drugs *in vitro*. However, the proposed system is not limited to adipose tissue, and the mentioned techniques to be demonstrated should provide a generic blueprint for virtually any *in vitro* tissue.

As these studies mature, we can anticipate that multiple tissue types will be integrated into one system, most likely by linking bioreactors or zones of connection within single bioreactors, allowing cross talk between different cell/tissue cultures. This would be a step forward in relevance related to drug kinetics and biological development that would expand the utility of the proposed aims. Since we have already shown that complex bioreactors can be designed to concurrently grow bone and cartilage tissues (Grayson et al., 2011), these future goals are realistic. Further, as the multitude of tissue types

successfully grown *in vitro* continues to expand, more diverse options will be presented for the types of drugs to be screened and tissues to be analyzed.

Background Information

An abundance of capital and labor has been invested into the research and development of more physiologically representative bioreactor technologies with improved monitoring capabilities (Figure 1A). Improved bioreactor systems allow for more clinically relevant research by engaging in less costly *in vitro* testing (relative to *in vivo*), while also providing a greater degree of control over the experimental environment.

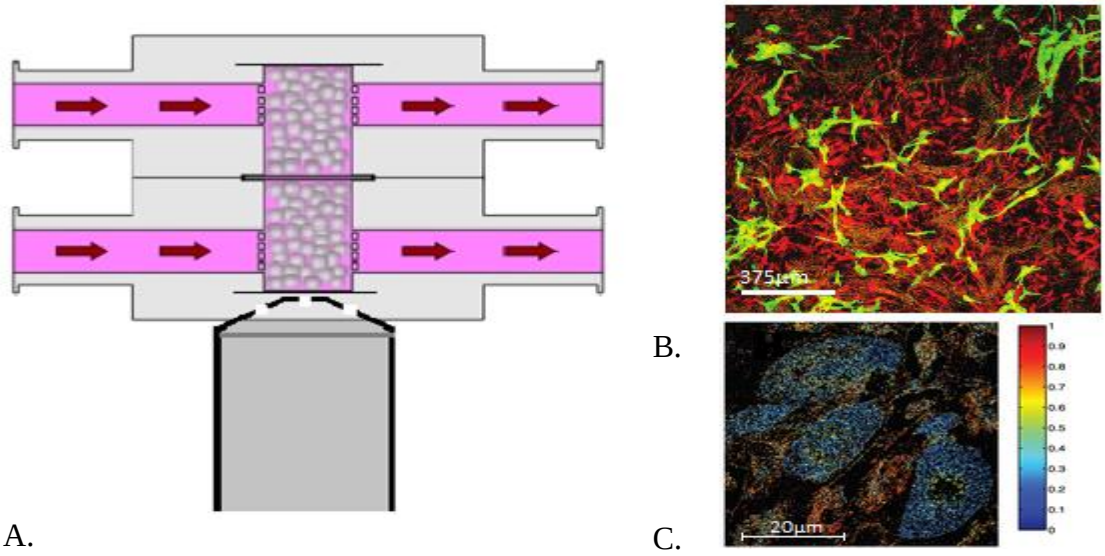

Figure 1. A) Bioreactor-imaging objective configuration to allow for both perfusion and imaging analysis of human tissues *in situ.* B) 3D confocal microscopy image of stained hASCs (red) and HUVECs (green) capable of being taken from bioreactor/imaging objective set up in (A) (Kang et al., 2009). C) Redox ratio image taken using TPEF imaging with a 63x objective that is capable of being taken from the configuration in (A). Ratio is calculated as [FP]/ ([FP] + [NAD(P)H]), and is inversely proportional to metabolic activity (blue represents high metabolic activity) (Rice et al., 2010).

To help in the aim of creating more physiologically relevant *in vitro* platforms through which to study cell and tissue behavior, the field of tissue engineering has expanded to include a more comprehensive and physiologically representative array of engineered human tissue protocols (Figure 1B). These tissues can serve as models for developmental biology, drug screening, and disease models.

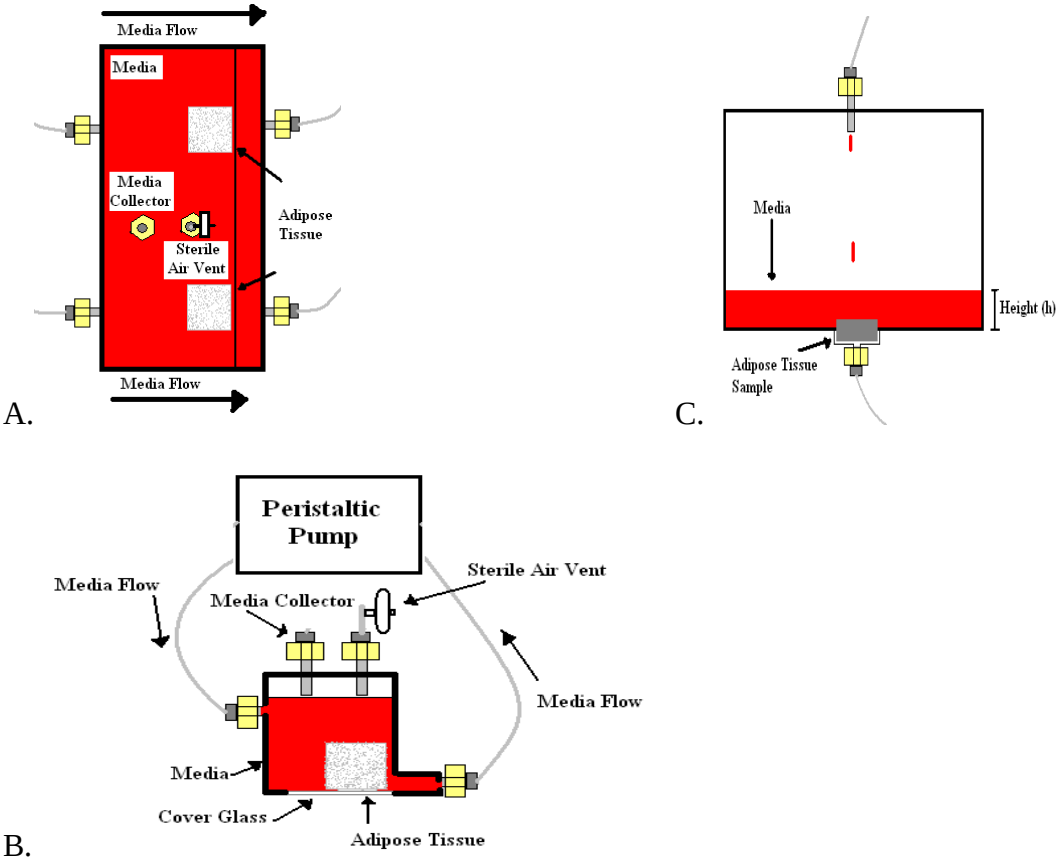

Figure 2. A) and B) Top and side views, respectively, of a possible bioreactor design to accommodate perfusion flow through an 8x8x8mm dimensioned adipose tissue construct, fitted with a cover glass imaging interface and media extraction capabilities. C) Schematic of an existing perfusion bioreactor within our lab that offers another direction for accommodating perfusion flow through a tissue construct.

To improve the means by which tissues are analyzed *in vitro* (and *in vivo* as well), research into advanced optical spectroscopic techniques and subsequent image processing methods have afforded researchers more tools with which to noninvasively monitor the morphology and metabolism of cells and tissues *in vitro* and *in vivo* (Figure 1C). The use of only endogenous fluorophores as sources of contrast improves the ease by which these analyses are done, and provide real time dynamic information on the metabolism and structure of the experimental tissue populations from within a bioreactor system. By combining all the elements described in Figure 1, it is feasible to design and build a novel bioreactor system to accommodate perfusion flow, media extraction, and noninvasive metabolic profiling through a cover glass imaging interface (Figure 2)

BIOREACTOR DESIGN

An inverted Leica confocal microscope with a 63x objective with a working distance of 0.57 mm will be used for the planned experiment. Attached to the same microscope will also be a 20x objective, where these magnifications are both along the same orders of magnitude as what has been previously used in adipose tissue imaging (Dicker et al., 2010). To achieve images throughout the tissue, the objective must be positioned within 0.2mm of the bottom of the sample.

To achieve this requirement, another recent system was designed to allow for continuous imaging of engineered human tissues and biomaterials from within a bioreactor at this working distance (Kluge et al., 2011). A Corning Cover Glass, 160-190 micron thick molded to a rectangular void on the bottom of the chamber was used successfully to

image cells, tissues and matrices in this prior system (Figure 3). The glass was press fit to a polydimethylsiloxane (PDMS) ring.

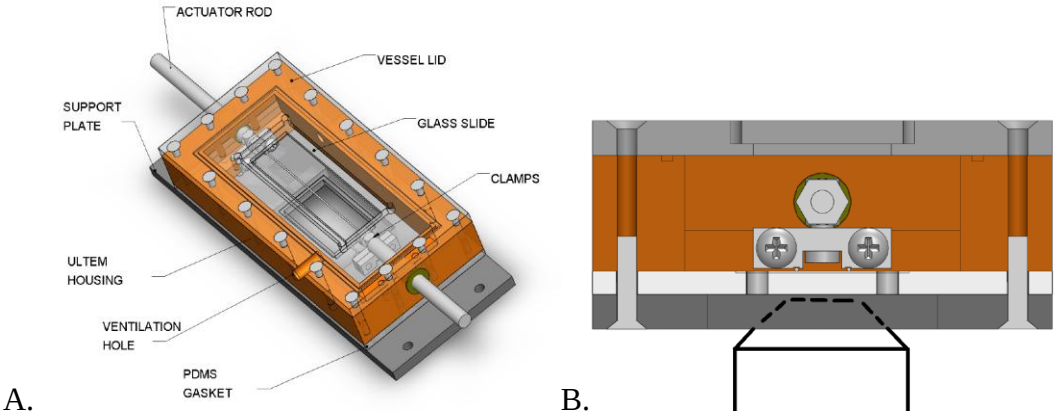

Figure 3. Previously designed bioreactor that utilized a cover glass in PDMS mold to continuously image human tissues and biomaterials from within a bioreactor (Kluge et al., 2011). A) Isometric view showing where cover glass is located with respect to rest of chamber. B) Side view showing how the objective of an inverted microscope will approach the cover glass and image the clamped biomaterial.

Previous bioreactor systems (Grayson et al., 2010; Kluge et al., 2011) have used PDMS gaskets to prevent leakage when tightening two hard, flat, machined surfaces to one another. The bulk materials used in these previously described bioreactors have been Polycarbonate and ULTEM because of their hardness, machinability, and autoclave-ability.

Perfusion bioreactor systems have also been described that were capable of achieving very controllable and constant flow rates using peristaltic pumping mechanisms made by MasterFlex (Grayson et al., 2010). No work has yet been done on optimal flow rates of engineered adipose tissue *in vitro*, but research has been published on the experimentally

derived optimum flow rates in the process of tissue engineering for human bone grafts from human adipose derived stem cells (Grayson et al., 2011). Lateral flow rates ranging from 80-1,800 μm/s were experimented with to determine which flow rates yielded optimal cell proliferation as measured through RT-PCR of bone specific markers. Flow rates of 400-800 μm/s were found to be optimal in promoting engineered bone tissue growth.

Other studies have shown different flow rates that have worked for their particular applications and tissues. Cardiac tissue has been grown by seeding myocytes and endothelial cells on channeled elastomeric scaffolds at a flow rate of 1 mm/s (Maidhoff et al., 2010). Another study has shown that adipose tissues from rats can be sustained in vertical flow bioreactors for ten days (Paaske 1973).These previous studies support the use of perfusion bioreactor systems, and provide some useful initial guidelines on flow rates.

IMAGING

The array of optical spectroscopic techniques that continues to be developed brings about the potential to noninvasively monitor the metabolic activity of cells using purely endogenous target molecules. A better understanding of the metabolism of cells within any particular tissue or organ system can provide insight into development, aging, pathogenesis, and drug response. By utilizing noninvasive techniques to metabolically profile intracellular activity, changes in metabolism can be monitored in real time. This provides more relevant information by allowing the metabolic progression of the same

tissue(s) to be monitored as a function of time. Through the use of purely endogenous targets in these imaging methods, metabolic profiling for the purposes of diagnosis and research can be expedited, and any variability involved in fluorescent marker specificity and the complications of exogenous fluorophores can be averted. A list of techniques commonly used to noninvasively monitor biological metabolism using entirely endogenous sources of contrast is shown in Table 2.

	Mechanism	**Information Acquired on Target Molecule(s)**	**Output**	**Type of Target Molecule(s)**
Fluorescence Lifetime Imaging	Fluorescence	Presence	False Color Map	Fluorophore
Redox Ratio	Fluorescence	Presence/ Concentration	False Color Map	Fluorophore
Electron Paramagnetic Resonance	Magnetic Electron Spin Resonance	Presence/ Concentration	EPR Spectrum	Free Radical

Table 2. Summary of the most commonly used imaging methods capable of noninvasively detecting changes in metabolism.

Currently, the metabolism of human tissues is most commonly studied through destructive and invasive techniques including but not limited to histology and assays. In these measurements metabolism itself is not often being measured directly. Instead, metabolism is being indirectly measured through staining the products and intermediates of metabolic processes, or by extracting biofluids from the system and performing assays or blot analysis. For the purposes of diagnosis, this is burdensome and invasive. For research purposes, this compromises the quality of the data obtained because no inter-

sample variability is accounted for (each sample being analyzed and providing data is immediately destroyed thereafter, and all data obtained from future time points have no direct relation to the previously obtained data).

Imaging has primarily served as a technique for understanding structural and morphological changes in human tissues. To understand how an in vivo or in vitro system is responding to a particular treatment, information on microenvironment changes with respect to both the bioenergetics and biochemical activity is essential. Imaging techniques offer the advantage of monitoring these dynamic changes as they occur in real time.

Understanding the level of activity and type of metabolic behavior occurring in human cells and tissues is paramount to both the diagnostic and engineering fields. Diagnostically, metabolism can indicate whether a particular pathology is developing, has developed, and the current stage. From an engineering perspective, understanding intracellular metabolism can help understand how a particular tissue is responding to a biomaterial, whether or not a sample of engineered human tissue sufficiently resembles its native counterpart, or whether a particular drug is having the desired effect or has become toxic.

When it comes to the possibility of using imaging modalities as a means for monitoring the metabolic behavior of a living cell/tissue system, the possibilities are only limited by the endogenous target molecules that can be detected through noninvasive methods. On a molecular level, the most successful methods by which metabolic intermediates and end products have been detected is through their characteristic electron orbital energy states (which reflect absorption and emission spectra) and spin orientations (reflecting

resonance).The two most successful molecular mechanisms by which noninvasive metabolic profiling has been efficacious are fluorescence and resonance spectroscopic methods.

Fluorescence Spectroscopy

The fundamental principle of fluorescence spectroscopy is the emission of light from a molecule after the absorption of light at a specific wavelength (Skoog et al., 2007). Fluorescence spectroscopy takes advantage of specific excitation/emission wavelength characteristics of endogenous molecules within biological cells and tissues to detect the presence and concentration of these molecules based on the wavelength and intensity of light emitted. Light of a chosen wavelength (excitation wavelength) is shone onto a biological sample which will absorb the light, then respond by emitting light at different intensities across certain wavelengths (emission wavelengths). Different endogenous molecules exist within organelles, cells, and tissues that are known to fluoresce at particular emission wavelengths when excited at specific excitation wavelengths. These molecules are known as fluorophores, and can be measured noninvasively using the principles of autofluorescence. A list of endogenous fluorophores is shown in Table 3 listing characteristic ex/em wavelengths and fluorescent lifetimes.

Through fluorescence spectroscopy, the key metrics that can be measured are the intensity of emitted light and the fluorescence lifetime of the sample. The intensity is simply proportional to the concentration of the particular fluorophore with excitation and emission wavelengths similar to the wavelength being used to excite the sample and

emission bandwidth being detected. The lifetime measurements however do not reflect concentration, but instead only reveal information on the temporal difference between excitation and emission of light energy from target molecules (Conklin et al., 2008). This value is dependent on the molecule's microenvironment, and so these measurements can also be used to detect pH, temperature, oxygen concentration, and protein binding (Provenzano et al, 2008).

	Excitation Wavelength (nm)	**Emission Wavelength (nm)**	**Fluorescence Lifetime (ns)**
NAD(P)H	340	450-470	0.3 (2 bound proteins)
Flavins	370, 450	530	5.2 (<1 bound protein)
Elastin	300-340	420-460	0.2-0.4 / 0.4-2.5
Collagen	300-340	420-460	0.2-0.4 / 0.4-2.5
Melanin	UV / Visible	440, 520, 575	0.2 / 1.9 / 7.9
Lipofuscin	UV / Visible	570-590	Multiexponential

Table 3. Endogenous fluorophores with their characteristic excitation/emission wavelengths, and microenvironment dependent fluorescence lifetimes (Koenig and Riemann, 2003). Notice the microenvironment dependence shown in the fluorescent lifetime measurements that in the cases of NAD(P)H and Flavins include protein binding.

Fluorescence Redox Ratio Analysis

Theory

When light of a particular wavelength is shone on a target fluorophore, the energy of the photons will be absorbed by the molecule, causing an electron of the target molecule to become excited to a higher energy state (Figure 4A). The electron will then slowly relax down to the lowest energy state of the orbital it was excited to before relaxing and emitting a photon back down to its former energy level at its ground state (lowest energy)

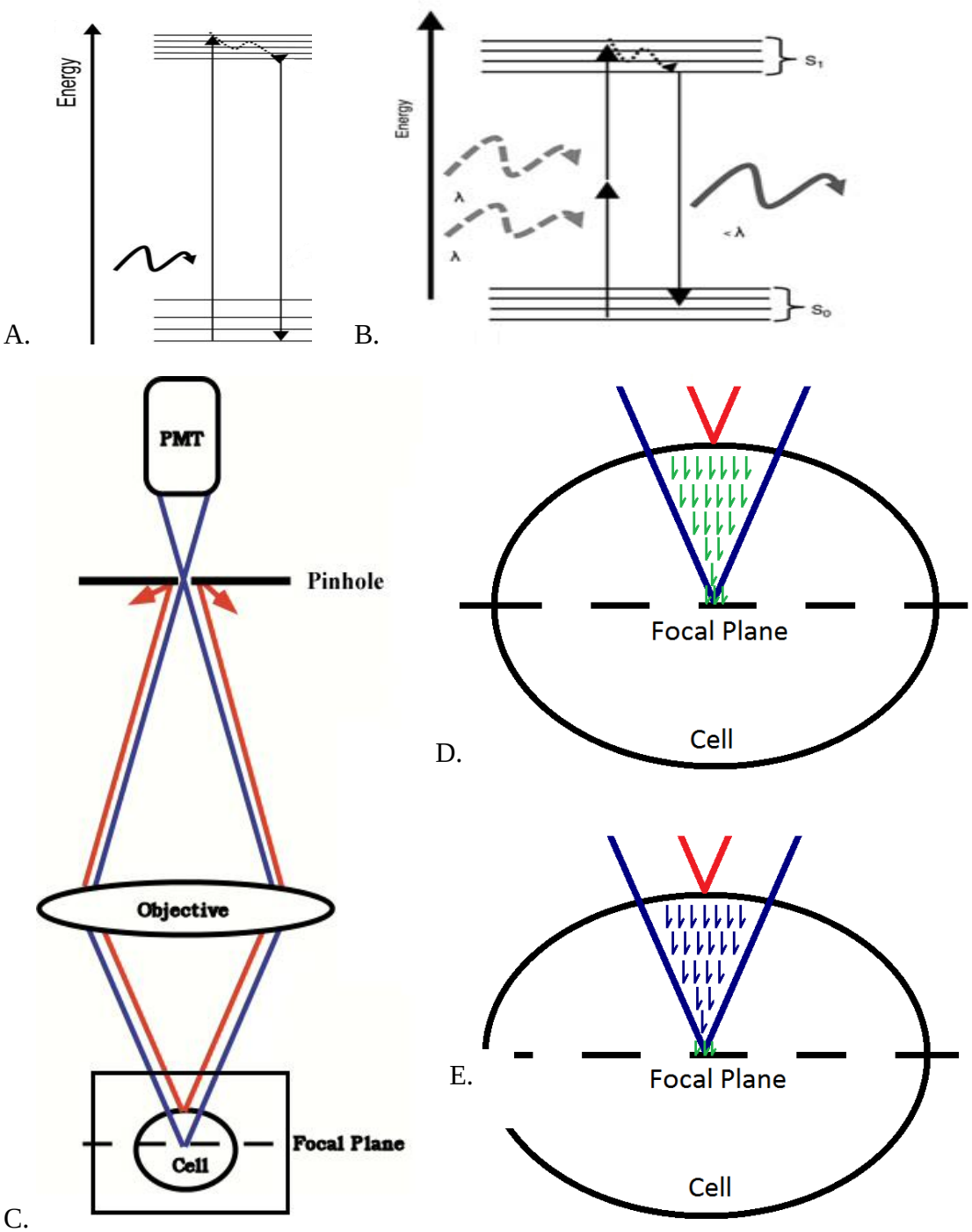

Figure 4. A) Linear fluorescence. B) Nonlinear fluorescence (TPEF). C) Principle of confocal microscopy using a pinhole to remove out of focus light. D) Linear fluorescence showing fluorescence (green arrows) occurring throughout cell between out of focus (red) and in focus (blue) light. E) Nonlinear fluorescence where fluorescence only occurs at the sight of in focus light on the focal plane (green arrows) but not elsewhere (blue arrows). Georgakoudi, et al 2008

(Georgakoudi et al., 2008). In the case of linear fluorescence microscopy, one emitted photon from the light source will be enough to excite the electron to its excited state and result in fluorescent events at a frequency that is proportional to the intensity of the laser light. In the case of nonlinear fluorescence microscopy (i.e., two photon excited fluorescence), multiple photons of a lower energy state (longer wavelength) will combine energies to cause the excitation of an electron to an excited state that otherwise could not have occurred with just one photon of the laser light (Figure 4B). In the case of nonlinear fluorescence, the fluorescent light which is emitted from the fluorophore is of a higher energy (shorter wavelength) than the absorbed light. This is the principle of multi photon fluorescence.

The detection of this light at different penetration depths to acquire image stacks within a tissue varies from linear to nonlinear microscopy. In the case of linear microscopy, depth resolved images are acquired at different depths by focusing the focal plane at the specific depth within the tissue and removing out of focus light through a pin hole at the detector (Figure 4C). The removal of out of focus light (red line) is necessary in linear microscopy because the excitation light will have sufficient energy to cause autofluorescent events throughout the cell (both out of focus and in focus light) and not just at the focal plane (Figure 4D). The resulting out of focus fluorescent events must therefore be removed through the pinhole. In the case of nonlinear fluorescence, the likelihood of the simultaneous absorption of two photons is significantly less than in the case of linear fluorescence (Georgakoudi et al., 2008). This is a result of the significantly smaller cross section values for two-photon excitation of endogenous chromophores

relative to the complimentary single-photon cross sections. Because of this lower probability, only the volume within the focal plane of the excitation light will have sufficient energy to allow for multi photon fluorescence to occur at a high enough frequency to be detectable (Figure 4E). As a result, no pinhole is necessary to achieve depth resolved images when using multi photon microscopy.

The laser light used to excite the sample and the emitted fluorescent light gathered through a detector can be filtered to allow for control over what fluorophores are being excited and what emission spectra are being measured. In the case of redox ratio analysis, the emitted fluorescent light gathered within a particular bandwidth can be analyzed using image processing to assign numerical values for the intensity of light gathered throughout the image (Rice et al., 2007; Quinn et al., 2011). By making sure the image is not saturated, information on the relative concentration of each fluorophore at each position within the image can be gathered. Using image processing, concentrations of fluorophores such as FAD and NAD(P)H can be gathered using the excitation and emission spectra shown in Figure 5. After assigning values to each pixel within the acquired image that reflects the intensity of each fluorophore at their respective emission spectra, the redox ratio per each pixel in the image can be calculated according to the formula:

$$\text{Redox Ratio} = \text{FAD}/(\text{FAD}+\text{NAD(P)H})$$

This redox ratio is widely used throughout the literature, and is known to be inversely proportional to anabolic activity (Rice et al., 2007; Skala and Nirmala 2010). FAD and NAD(P)H are both common intermediates in many energy consuming/releasing

metabolic pathways. Their expression is in primarily within the mitochondria of the cell during the processes of glycolysis, citric acid cycle, and oxidative phosphorylation. In anabolic situations where NAD(P)H is being produced in high quantities as a result of glycolysis and the citric acid cycle operating, then the redox ratio will decrease (i.e., lipogenesis). However, in anabolic situations in which NAD(P)H is being rapidly consumed along the electron transport chain (even if glycolysis and the citric acid cycle are running), then the concentration of NAD(P)H will decrease, causing an increase in the redox ratio (i.e., high energy demand cells like cardiomyocytes).

Ex/Em (below/right)	525nm	400nm
755nm	NAD(P)H/FAD	NAD(P)H
860nm	FAD	Lipofuscin

Figure 5. Excitation (755/869) and emission (525/400) spectra of the fluorophores NAD(P)H and FAD.

Applications

Changes in the redox ratio can represent changes in the metabolic activity in a cell, which is known to elevate during differentiation, cell division, cancer, and catabolism (Zhuo et al., 2010). Being able to observe changes in the redox ratio through imaging has applications in being able to characterize different environments, treatments, and ongoing conditions within cells of different tissues noninvasively. This work has been used to track cellular differentiation status (Figure 5) and 3D adipose tissue growth *in vitro* (Rice et al., 2007; Quinn et al., 2011).

A.

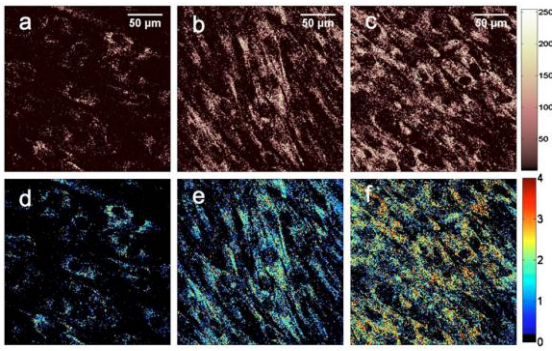

B.

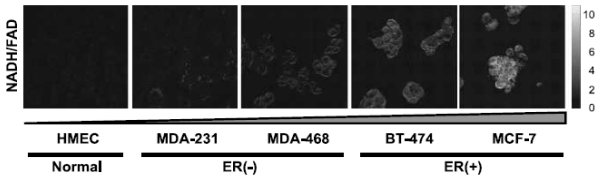

Figure 5. A) Top three images are two photon excited fluorescence images collected at 455nm for human mesenchymal stem cells differentiating into adipocytes. Bottom three images are false color redox ratio maps of the corresponding upper images (Rice et al., 2007). B) Redox ratio images comparing normal mammary epithelial cells to different breast cancer cell lines (Ostrander et al., 2010).

As a noninvasive means for monitoring human tissues, redox ratio analysis through multi photon imaging has also been researched as a technique for diagnosing skin disease *in vivo* (Zhuo, et al 2010). Cancer is known to increase metabolic activity, and so a decrease in the calculated redox ratio can be used to diagnose skin cancer. As seen in Figure 5B, other research has built on this possibility and shown the potential of using redox ratio analysis to differentiate between breast cancer and normal cell lines *in vitro* (Ostrander, et al 2010).

Fluorescence Lifetime Imaging

Fluorescence lifetime imaging (FLIM) is a noninvasive imaging technique that measures the time required for an excited fluorophore to relax back down to its stable state. This is helpful when redox ratio analysis gathered through two photon excited fluorescence imaging doesn't sufficiently differentiate between the fluorescent sources of different molecules. In these cases, FLIM can be used to measure the time required for excited molecules to relax, which is often different for different fluorophores, and dependent on microenvironment, pH, and temperature (Provenzano et al., 2008).

Theory

The key measurement behind FLIM analysis is the measurement of the time difference between the absorption and emission of light from fluorescing molecules. In order to target specific relevant fluorophores while not photo damaging the tissues, TPEF imaging is often used for FLIM (Provenzano, et al 2008). Given a target fluorophore, light at a specific wavelength is shone onto a tissue where it is absorbed by a target fluorophore, exciting it to an excited state energy level. The excited electron within the target fluorophore will then emit fluorescent light as it returns to its ground state level (Figure 6A). The time between the absorption of the excited light and emission of the fluorescence light is known as the fluorescence lifetime of the sample (Conklin et al., 2009).

The behavior of the fluorescence lifetime of a population of fluorophores is that of a decay. A laser pulse width of 100fs can pulse on a sample at a frequency on the order of

100MHz, exciting a fluorophore which then leads to a considerably longer fluorescence lifetime decay (Figure 6B). This data can be represented in either frequency or time domains depending on the analysis.

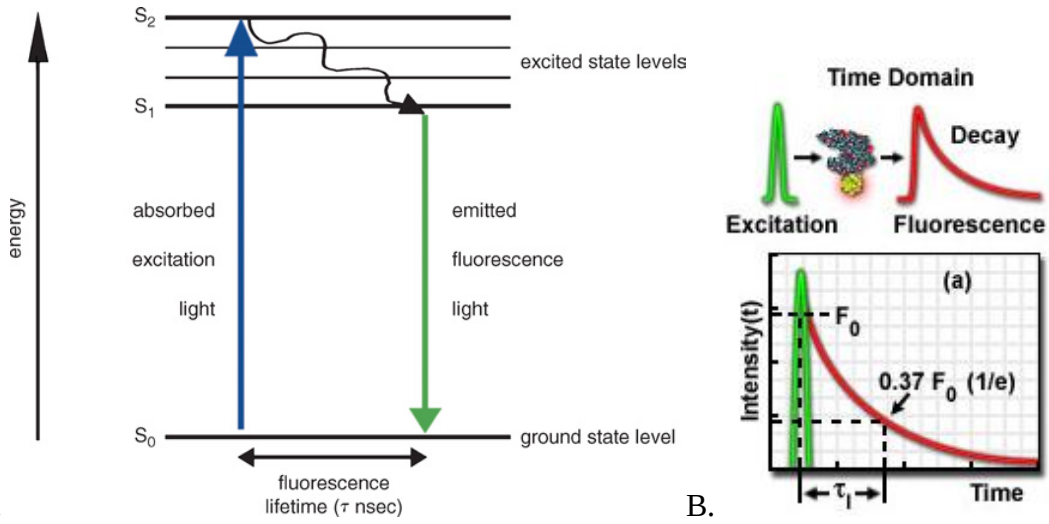

Figure 6. A) Schematic definition of fluorescence lifetime with respect to absorption and emission of light (Lleres and Swift 2007) B) Graphical representation of the fluorescence decay lifetime after initial excitation.

The fluorescence lifetime of a particular fluorophore is usually measured using a time correlated single photon counting (TCSPC) module operating at picoseconds resolution capable of collecting data at either singular or multiple emission wavelengths. This equipment can be commercially bought by vendors including but not limited to Beckr & Hickl. The TCSPC module is then connected to a photomultiplier tube (PMT) in order to amplify the signal gathered by the TCSPC module. The output data is then specifically a reflection of the fluorescence lifetime of the sample being imaged at the excitation wavelength being used and emission bandwidth being detected. Unlike traditional

fluorescence measurements, FLIM measurements are independent of fluorophore concentration, allowing for improved differentiation between different fluorophores which may have similar emission spectra at the same excitation wavelength, but differing fluorescence lifetimes (Provenzano et al., 2008). However, in some cases there will be fluorophores with similar fluorescence lifetimes at particular excitation, and so in these cases it is always useful to supplement FLIM with traditional fluorescence imaging to get an idea of fluorophore concentrations at different emission wavelengths.

Applications

FLIM is particularly useful when used alongside traditional fluorescence imaging because FLIM takes advantage of the same excitation/emission characteristics of target fluorophores, and is simply just a different means by which to analyze and interpret the information gathered by the emission spectra. This is helpful when redox ratio analysis gathered through TPEF imaging doesn't sufficiently differentiate between different sources of fluorescence from different molecules. In these cases, FLIM can be used to measure the time required for excited molecules to relax, which is often different for separate fluorophores, and dependent on microenvironment, pH, and temperature. Because of this, the fluorescence lifetimes of common fluorophores measured in fluorescence microscopy can be mapped out in the same way as the fluorophore excitation and emission wavelengths, as shown in Figure 7 (Koenig and Riemann 2003).

This is especially useful for fluorophores that have overlapping emission spectra at similar excitation spectra (i.e., Melanin and Lipofuscin, from Table 3). With FLIM, it is

now possible to distinguish the presence of melanin in diseased verses non diseased tissues while in the presence of fluorophores with similar fluorescence spectra (lipofuscin), and has been used to image for the presence of malignant melanoma through FLIM-sensitive sources of contrast within the same focal plane (Koenig and Riemann 2003).

Because collagen in many environments is considered non-fluorescent (second harmonic generation is not necessarily fluorescence), it can be assumed in most cases that collagen has a fluorescent lifetime of zero. This has been used in the study of breast cancer to analyze tumor/stromal interactions because collagen can then be separated out from the tumor when imaging using the differences in their fluorescent lifetimes (Provenzano et al., 2008).

Two of the most common fluorophores used as a metric for metabolic activity are the metabolic intermediates NAD(P)H and FAD, both of which play integral roles in the electron transport chain of glycolysis and the citric acid cycle. Because both of these cycles occur primarily within the mitochondria of cells, FLIM has been used to distinguish mitochondria from within the cytosol and differentiate it from other organelles by targeting biochemical cues (NAD(P)H and FAD). And because FLIM can also be used to detect structural features, it can therefore be used to differentiate different features as a function of their different structural and biochemical attributes (Figure 7B) (Koenig and Riemann 2003). FLIM analysis of NADH fluorescence has shown that the fluorescent lifetime of NADH will change as a function of pathogenesis, maturity, and cell density (Ghukgasyan et al., 2009). The fact that the fluorescent lifetime of NADH changes as a function of cell density suggests that cell-cell interactions are likely another

microenvironment factor that affects the fluorescent lifetimes of biomolecules. Because the molecule of NADH has not changed, this data implies that the microenvironment in which the NADH is present has changed as a result of the aforementioned metabolic changes, representing an example of how FLIM analysis can be used to track intracellular changes noninvasively.

Utilizing FLIM with TPEF on a confocal microscope also provides the ability to acquire fluorescence lifetime images at varying depths within a tissue. This is more relevant for layered tissues, like skin, where the fluorescence lifetime measurements coupled with fluorescence intensity imaging have been used to detect the presence or absence of different fluorophores at varying dermal and sub dermal layers in diseased vs. non diseased tissues (Lee et al., 2009). The unique fluorescent lifetime data acquired for fluorophores at the distinct layers within skin tissue allows for a very precise noninvasive technique for assessing the metabolic activity and overall health of skin tissue. The fluorophores most common within skin that contribute to the FLIM measurements are keratin, NAD(P)H, melanin, elastin, and collagen provides SHG (Breunig et al., 2010). Each of these endogenous molecules has characteristic ex/em spectra and is found at varying concentrations in different microenvironments within each layer of the skin dependent on the metabolic and structural state of the skin. Cataloguing the FLIM measurements normal to healthy skin could be used for either diagnostic purposes or tissue engineering applications where FLIM analysis could be used to determine if a tissue engineered skin sample is alike to its natural counterpart, and in what layers it fails to match up.

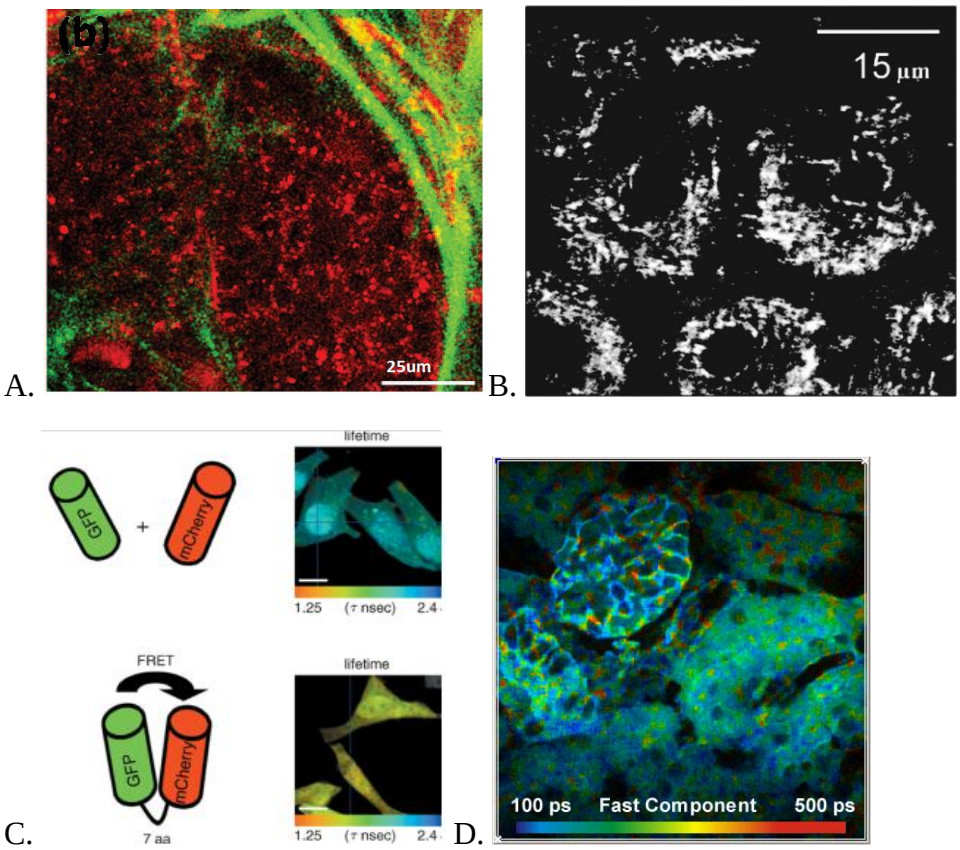

Figure 7. A) Live mammary tumor tissue with separated with fluorescence/second harmonic generation (SHG) signals separated by FLIM measurements taken at an excitation wavelength of 890nm. Green is false colored collagen (SHG). Red is false colored tumor tissue (FLIM). B) Isolation of different intracellular organelles based on the principles of FLIM. The dark spots within these cells are non-fluorescent nuclei (Koenig and Riemann 2003). C) FLIM measurements showing the differences between the bound and unbound forms of GFP and mCherry proteins (Lleres and Swift 2007). D) False color showing advertised capabilities of Becker-Hickl SPC150 TCSPC module.

As mentioned earlier, protein binding can also result in a change in the fluorescence lifetime of an endogenous molecule. NADH has shown to express different lifetime measurements as a result of protein binding (Ghukgasyan et al., 2009), and a proof of concept has been further demonstrated using an exogenous mCherry molecule binding to GFP (Figure 7C) (Lleres and Swift 2007). Through this, FLIM measurements can also provide for information on protein-protein binding *in vitro* and *in vivo*. The output can

then be displayed as a false color mapped image representing the fluorescence lifetimes determined per each pixel in the acquired image (Figure 7D).

However, as mentioned before, the fluorescence lifetimes of various fluorophores is not constant, and does change as a function of the fluorophore's microenvironment (pH, oxygen content, temperature, the presence of binding molecules, and fluorescence resonance energy transfer) (Roberts et al., 2011). Using this principle, FLIM can also be used to analyze the biochemical environment in which a specific fluorophore is. The fluorescence lifetime of a fluorophore has been shown to change as a result of binding to another protein, and this analysis has allowed for the detection of protein-protein interaction using FLIM (Lleres and Swift 2007).

Resonance Spectroscopy

Resonance spectroscopic methods can be subdivided into two groups, nuclear magnetic resonance (commonly NMR) and electron paramagnetic resonance (EPR). Both of these approaches have shown promise with both *in vitro* and *in vivo* applications for understanding the presence and concentrations of particular molecules to understand morphology, pathology, and most importantly metabolism (Vanea et al., 2008). NMR spectroscopy takes advantage of the magnetic properties of molecular nuclei and obtains a signal proportional to the free concentration of particular compounds across a range of radiofrequencies and magnetic field strengths (McCully 1999). This can be used to determine the presence of certain isotopes in an *in vitro* or *in vivo* setting. However, varying levels of interference caused by endogenous metabolites that obscure the signal

of target metabolites often results in a need for extraction of specific biofluids or biosolids from their *in vivo* environment to effectively analyze them (Lenz 2011). Because of this, NMR spectroscopy is not the most effective means by which to noninvasively profile the metabolic activity of an *in vivo* environment, and so will not be a large focus of this paper.

Electron Paramagnetic Resonance Spectroscopy

Theory

Electron Paramagnetic Resonance (EPR) spectroscopy exploits the intrinsic magnetic moment of unpaired electrons that arise from their different spin orientations (Spasojevic et al., 2011). An exogenous magnetic field is applied to the population containing unpaired electrons, and the electrons will then either align with or in the opposite direction of the magnetic field (Figure 8A). An EPR spectrometer measures changes in energy absorption in a particular sample as a function of the presence of different paramagnetic species. The output signal reflects the presence of and information about the paramagnetic species present within the sample as a result of being subjected to an exogenous magnetic field (Figure 8B) (Kadantsev and Ziegler 2010). Electrons can be coupled to one or multiple nuclei. This information will be reflected in the output EPR signal which is dependent solely on the unpaired electron's interactions with the nuclei around it and its characteristic spin.

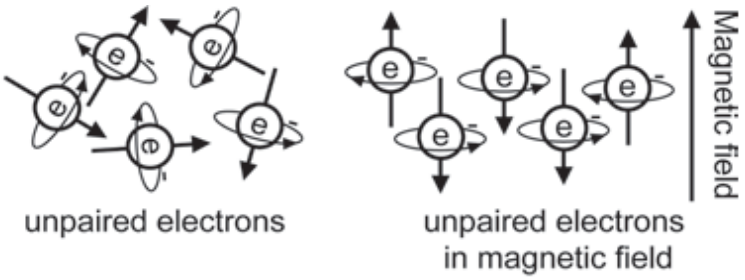

A.

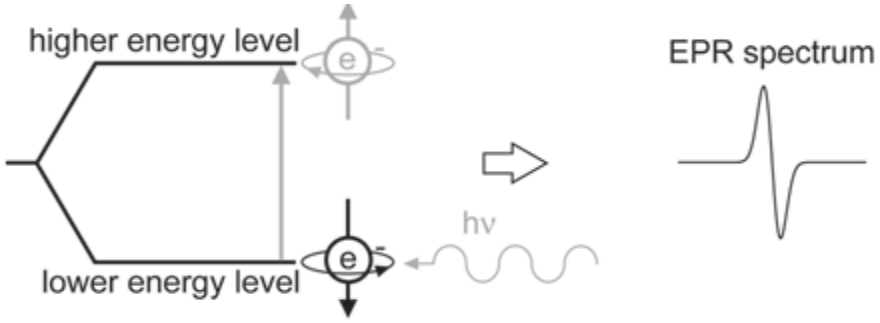

B.

Figure 8. A) After an exogenous magnetic field is applied to a cellular microenvironment with molecules containing unpaired electrons the spins of the electrons will then either align with or in the opposite direction of the magnetic field. B) Dependent on whether or not the unpaired electrons align with or opposite of the magnetic field direction will be reflected in the output of the EPR spectrum signal.

Two methods are often employed for the use of EPR spectroscopy; spin trapping of short lived radicals, and EPR spectroscopy of more stable paramagnetic endogenous molecules (Spasojevic 2011). Both utilize the same EPR spectroscopic theory described above, but spin trapping instead focuses on short lived radicals whose unpaired electron is more easily noticed when the molecule is bound to another endogenous molecule resulting in what is known as a spin adduct. The spin adduct is considerably more stable and still exhibits free radical behavior and detection with a unique signal during EPR spectroscopy.

Applications

The spin trapping method has been used to detect as an EPR spectroscopic method to detect and characterize free organic radicals for the detection of nitric oxide (Wilcox and Smith 1995; Fujii and Yoshimura 2000). Hemoglobin (Hb) has commonly been used as the compound that reacts with the free nitric oxide radical (NO) to form the stable spin adducts which has a well characterized Hb-NO EPR spectra.

Reactive oxygen species (ROS) are free oxygen radicals that contain an unpaired electron. They arise naturally during the process of oxidative metabolism where free electrons are often leaked out of the electron transport chain onto molecular oxygen in the mitochondria. ROS have been shown to regulate enzyme activity through a series of pathways known as redox signaling (Rhee 1999; Spasojevic 2011). Because EPR spectroscopy only detects molecules with unpaired electrons and the output signal is entirely dependent on the presence of unpaired electrons and their reactions with surrounding nuclei, EPR spectroscopy can be used to detect and differentiate between ROS, NO, NADH dehydrogenase, ascorbyl radical, tocopheroxyl, melanin, and others (Fujii and Yoshimura 2000; Spasojevic 2011; Albracht 2010). Each of these radicals has been shown to produce unique EPR signals allowing for both their presence and concentrations to be measured noninvasively *in vivo*, *in vitro*, and *ex vivo* (Fujii and Yoshimura 2000).

Application of high resolution pulsed EPR techniques have been shown capable of providing highly detailed structural information on transient paramagnetic molybdenum centers of different organisms (Hanson et al., 2010). This resolution has not yet been shown to, but could be used to differentiate between different antioxidant buffers at the

interface between different intracellular organelles to gain a better insight of the behavior (or potential) of redox signaling as a function of intracellular location.

Redox Signaling

The redox signaling that EPR spectroscopy enables the user to observe is an indicator of redox activity and what is occurring metabolically within a particular compartment of a cell. Superoxide anions have been shown to be directly linked to oxidative phosphorylation during mitochondrial respiration (Leloup et al., 2011). And although the mitochondrion are known to be the primary source of redox signaling detection, redox signaling also exists and can be detected across different intracellular compartments like the endoplasmic reticulum and cytosol (Leloup et al., 2011).

The growth and development of many aerobic organisms relies heavily on the presence of ROS. ROS react strongly with redox compounds such as NAD, NADP, glutathione, and ascorbate (plants), all of which signal an increase in metabolic activity and are paramount to understanding bioenergetics processes (Noctor 2006). The redox reactions which can be measured through EPR as a function of ROS concentration are fundamental to the development and maintenance of cells, and provide information on how energy is allocated throughout the different compartments of the cell.

Further analysis has shown redox signaling to be indicative of gene expression by measuring NAD+/NADH ratios, where exogenous interference of the redox compound ratio has been shown to inhibit the gene expression (Yu et al., 2009; Noctor 2006). The presence of antioxidants within a cellular microenvironment have also been shown to

have an effect on redox signaling, influencing growth, development, cell elongation, mitosis, senescence, and apoptosis (Pavet 2005). Antioxidants therefore exist at varying concentrations within separate organisms and in the interstitial intracellular space between them to act as a buffer to accommodate the optimal redox signaling.

Conclusion

Because of interference amongst molecular nuclei in any biological sample, the most exploited methods used to noninvasively detect metabolic intermediates and byproducts to assess metabolic activity in biological samples take advantage of the electronic energy levels and spin orientations of the molecular targets. Fluorescence spectroscopy and resonance spectroscopy utilize these electronic states of metabolic compounds to measure metabolic activity in living human tissue samples both *in vivo* and *in vitro*. Fluorescence spectroscopy allows for both fluorescent lifetime imaging and fluorescence redox ratio analysis. Fluorescence lifetime imaging provides information on the presence of particular fluorophores and is known to vary with changes in the microenvironment of the focal plane. This way, FLIM can offer information not only on the presence of a particular fluorophore, but also the environment it is in. Redox ratio analysis provides information on the presence and concentration of particular fluorophores within a certain focal plane, and uses image processing techniques to compare the relative concentrations of particular metabolic intermediates to assess the magnitude of metabolic activity present which can be increased or decreased as a function of differentiation, cell division, drug treatment, and pathology. Resonance spectroscopy is most useful in profiling biological tissue metabolism when used to measure the resonance of different electron

spin states rather than nuclear resonance. Electron Paramagnetic Resonance imaging provides information on the presence and concentration of different free radicals that exist during specific metabolic processes (i.e. oxidative metabolism).

The improvement of these noninvasive methods by which metabolic activity can be analyzed through purely endogenous sources of contrast provides a more convenient and scientifically efficacious method to characterize metabolic behavior *in vitro* and *in vivo*. The applications for this research exist both in diagnostics and research. The ease by which human tissues is studied is not only improved by being both noninvasive and relying on endogenous molecular targets, but the real time dynamic data that can be gathered improves the relevance of any data obtained in this way.

DRUG RESEARCH

The noninvasive tools used to profile metabolism via endogenous fluorophores outlined above have the ability to be turned towards pathological metabolic research, with particular applications in the field of drug development and screening. As mentioned before, the metabolic state of any particular cell is often affected by different pathologies, and then again by subsequent drug treatments.

In the case of adipose tissue, the two most heavily researched ailments are diabetes and obesity. Within these two conditions there is an eclectic variety of FDA approved drugs on the market with highly characterized and documented pharmacodynamic and pharmacokinetic effects with respect to cell and tissue metabolism and morphology. However, with the exception of a rare few, the majority of anti-obesity drugs tend to

focus either on stifling appetite, hindering absorption of certain fats, or increasing the patient's energy. Since the planned adipose tissue model will not include a digestive tract, drugs that speed up the breakdown of human fat tissue would need to directly act on adipose tissue, such as Methotrexate, a known tumor necrosis factor-α inhibitor which works by alleviating inflammation in adipocytes by decreasing leptin secretion and increasing adiponectin secretion (Gambero et al., 2011). However, it is still easier to consider antidiabetic drugs such as Thiazolidinediones, Sulfonylureas, Meglitinides and Sulfonylureas. The latter two are both known to act on, among other things, the K-ATP channels of cell membranes and have been associated with significant and sometimes dangerous increases in intracellular calcium ions (Kumar et al., 2008). These anti-diabetic drugs are easier to experiment with in the proposed model because they target adipose tissue directly unlike most anti-obesity drugs. A list of two Thiazolidinediones (Rosiglitazone and Troglitazone) plus insulin and norepinephrine with their corresponding effects (up or down-regulation) on significant adipose tissue biomolecules is shown in Table 4.

Thiazolidinediones (TZDs) are a class of insulin sensitizing drugs used primarily in the treatment of type 2 diabetes. Patients with type 2 diabetes are resistant to the effects of insulin, a hormone which is responsible for regulating the metabolism of glucose in the body. Without enough insulin, or in the case where a body is naturally resistant to insulin, glucose levels will rise in the blood because of the body's inability to metabolize it, and the body will begin to burn fat storages as a replacement by breaking down triglycerides in white adipose tissue.

	Rosiglitazone	Troglitazone	Insulin	Norepinepherine
Hormone Sensitive Lipase (Lipolysis Marker)	↑		[Insulin] Dependent	↑
Lipoprotein Lipase (Lipogenesis Marker)	↑		↑	
TNF-α Secretion	Not Significant		↑	
Glycerol Release	↑		↑	↑
Plasma [FFA]	↑	↑		
Acyl CoA Dehydrogenase Protein	↑	↑		
Adiponectin	↑			

160-200um **Table 4.** Up and down-regulation of various adipose tissue markers and biomolecules as a function of the delivery of Rosiglitazone, Troglitazone, Insulin, and Norepinephrine. Adiponectin is shown in bold because its upregulation by Rosiglitazone was shown *in vivo* only, whereas the other biomolecules have had their regulation characterized *in vitro* (Kim, 2004; Boden, 2005; Chao 2000; McTernan, 2002; Kahn, et al 2005)

For any particular drug to be considered an appropriate candidate for research with regards to profiling its effects on adipose tissue through noninvasive analysis, it should be a clinically relevant, FDA approved drug (with known biochemical mechanisms of action that are well understood and have been previously mapped out), and must have its actions shown to work directly and specifically on adipose tissue itself. Only then, can its mechanism of action be correlated to and validated by noninvasive metabolic profiling.

Drug Mechanisms and Functions

TZDs are known to be ligand agonists of peroxisome proliferator-activated receptor γ (PPARγ) and it is generally accepted that their insulin sensitizing abilities are carried out via their strong affinity towards PPARγ (Boden et al., 2005). Although the exact biochemical pathway that describes the mechanisms by which TZDs specifically affect adipose tissue has never been fully mapped out, the effects TZDs have on free fatty acids (FFAs), leptin, tumor necrosis factor-α (TNF- α), glucose, and insulin levels in the blood

plasma have been carefully researched for their applications as an anti-diabetic (schematic shown in Figure 9). TZDs effects on lipolysis/lipogenesis also provide insight into the metabolic effects TZDs have on adipose tissue.

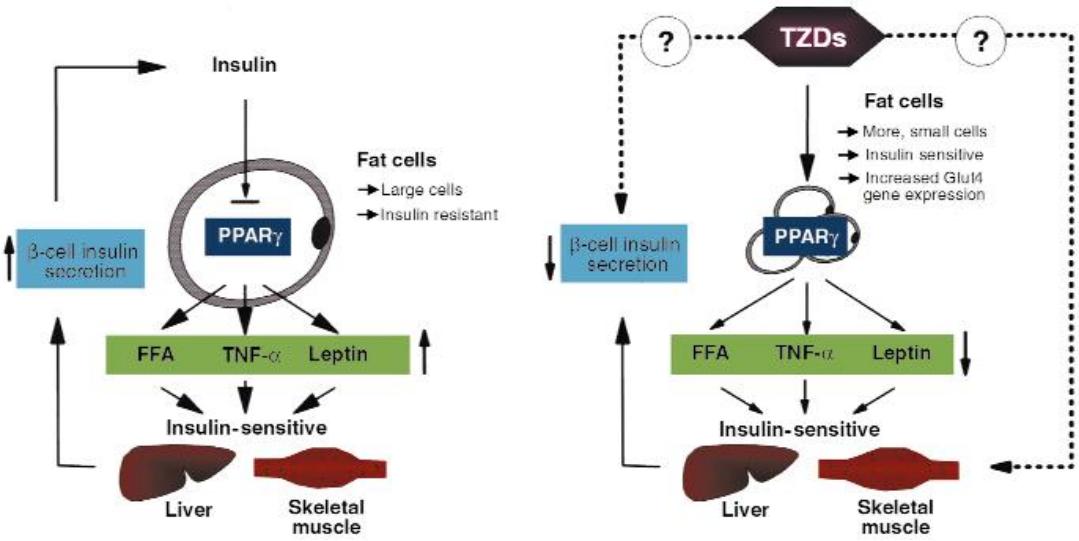

Figure 9. Left: Schematic describing relationship between adipocytes, organs, and insulin in the case of type 2 diabetes. Right: Similar schematic of type 2 diabetic system, only with the introduction of TZDs (Kahn et al., 2000). TZDs will decrease cell size, increase cellular proliferation, increase insulin sensitivity, and down regulate leptin, FFAs, and TNF-α.

In obese rats, it has been shown that the controlled delivery of rosiglitazone and darglitazone (two different types of TZDs) can decrease the triglyceride, insulin, and glucose content in the rat's blood plasma significantly (Oakes et al., 2001). This decrease in glucose shows an increase in the body's ability to metabolize glucose and convert it into energy. The TZD, rosiglitazone, was shown in another study to decrease the amount of FFAs in wild type mice after 5 weeks of controlled delivery (Chao et al., 2000). It has also been shown that TZDs, in restoring normal insulin sensitivity levels to adipocytes,

will as a result cause a simultaneous decrease in adipocyte size, providing a morphological cue for the effects of TZD administration (Kahn et al., 2000).

In another study, human white adipose tissue was removed from healthy patients during a biopsy, and experimented on in response to the delivery of the Rosiglitazone (RSG, a type of TZD) to the tissues *in vitro*. The administration of RSG to the tissue samples showed marked increases in lipoprotein lipase (LPL), a marker for lipolysis (Kirkpatrick et al., 2005). Delivery of RSGs also showed a net mass gain in the tissues, due to a concurrent increase in the rate of lipogenesis that surpassed the increase in lipolysis, implying a significant increase in adipocyte lipid metabolic functions. RSGs were also shown to increase the rate of pre-adipocyte differentiation into mature adipocytes during testing (Mcternan et al., 2002; Olefsky 2000).

Specificity Toward Adipose Tissue

However, for any of these reactions to TZD administration to be useful for a 3D tissue engineered model, it must be shown that these effects of TZDs are due to their direct interaction with adipose tissue. There is no use in testing with TZDS on engineered adipose tissue if their effects on adipose tissue are a result of watered down side effects caused by other changes and reactions TZDs incur elsewhere in the body that just happen to indirectly affect adipose tissue as well. As mentioned before, it is known that TZDs function as a ligand agonist for PPARγ. PPARγ is a nuclear receptor protein that is present not only in adipose tissue, but also skeletal muscle. However, it has been shown through the use of transgenic mice models, genetically modified at the adipocyte-specific

aP2 promoter gene so that no subcutaneous or intra-abdominal adipose tissue could be observed, that the effects of TZDs are overwhelmingly mediated via direct interactions with adipose tissue (Kahn et al., 2000). At maturation, the mice in this model all exhibited hyperglycemia, hyperlipidemia, and hyperinsulinemia. Normal levels of TZD administration (those that would be given to normal, fatty mice) showed no improvement on these ailments. It required an immensely larger administration of TZDs to the mice to cause lipid, insulin, and glucose levels in the mice to reach healthy levels. This is expected, since PPARγ is present in skeletal muscle and other tissues besides just adipose tissue. However the considerable increase in TZD dosage required incurring the same response in the absence of adipose tissue lends itself to the conclusion that the effects of TZDs are primarily realized by their interactions directly with adipose tissue.

In summary, the net effects of TZDs on FFAs, insulin, glucose, and lipid content in plasma can be directly accredited to the drug's interactions specifically with adipose tissue (Oakes et al., 2001; Chao et al., 2000). Rosiglitazone has been shown to cause a significant increase in the metabolic activity of adipose tissue via its direct interactions with adipocyte and adipose ECM. The metabolic activity brought on by rosiglitazone's interactions with adipose tissue has both anabolic and catabolic components. The rates of both adipocyte lipogenesis and lipolysis increase with rosiglitazone administration (resulting in a net increase in adipose mass). Rosiglitazone also increases the rate of differentiation of pre-adipocytes into mature adipocytes (Mcternan et al., 2002; Olefsky 2000). TZDs will also affect cell morphology, as the increased insulin sensitivity that TZDs impose on adipocytes has shown to decrease the cell's size (Kahn et al., 2000). These morphological, biochemical, and physiological effects that TZDs have been

reported to have on adipose tissue make them a strong candidate for drug screening using a 3D vascularized human adipose tissue model.

Correlate Drug Effects with Imaging

In order to continuously monitor the changes in adipose tissue in a non-destructive and non-invasive manner, the morphological and biochemical changes in the cells/ECM of the engineered adipose tissues must be correlated properly with the changes observed using advanced imaging techniques that are able to quantitatively measure the drug's effects as a function of the varying dosage volumes of the drugs being delivered (or no drug delivery). The challenge faced by the imaging tasks proposed here is following these changes in a 3D environment. Most drug screens analyzed via imaging methods are conducted in 2D cultures. Just viewing the adipocytes and ECM in 3D for qualitative analysis alone will require depth resolved images taken using confocal microscopy. In order to gain quantitative insight into the metabolic activities, lipid accumulation, etc., occurring in the engineered white adipose tissues will require even more sophisticated imaging techniques.

As mentioned before, the delivery of rosiglitazone to adipose tissue will cause an increase in both adipocyte lipid metabolism and the rate at which stem cells are able to differentiate into mature adipocytes (Mcternan et al., 2002). It has been shown in previous experiments that metabolic activity and differentiation status can be assessed in hMSCs subjected to adipogenic differentiation medium by use of two photon excitation fluorescence (TPEF) (Rice et al., 2007; Rice et al., 2010). During high levels of anabolic

activity, including lipogenesis, NADPH will be generated through both glycolysis and the citric acid cycles in order to generate citrate, which is exported from the mitochondria and used to create FFAs (which serve as precursors to lipid droplets). This increase in NAD(P)H will cause a decrease in the redox ratio. By being able to gauge the relative concentration and activity in cells, insight can be gained to the levels of metabolic activity going on in a particular cell culture using the redox ratio techniques described before.

Further image processing can provide insight into the morphological effects of RSG on adipocytes by calculating relative cell sizes and volume metrics between tissues subjected to RSG and control samples. This imaging technique gives biochemical and morphological cues as to what is going on in the cells, and can give insight into the growth and differentiation status of the cells in medium.

Rosiglitazone

Because RSG is known to elevate rates of metabolic activity, the redox ratios can be used to gauge the effects of different dosages of RSG and how they will affect the tissue samples (pharmacodynamics). Different methods of drug delivery to the tissues including but not limited to a single bulk delivery of one dose of RSG (simulating single intravenous bolus delivery), or prolonged delivery of smaller dosages of RSG to the tissues over time (could simulate multiple injections, or repeated oral deliveries) can then be compared and studied with respect to one another by visually monitoring the metabolic activity of the tissue via the aforementioned redox ratio. By varying the

dosage sizes, the toxic and therapeutic thresholds can also be determined so as to better understand at what concentrations the drug should be supplied to adipose tissue. And although the proposed 3D tissue system will consist of only adipose tissue and no renal or hepatic system to filter out the drugs, insight can be gained as to what the 'staying' power of the drugs are in the local adipose tissue system before the drug is degraded and its effects discontinue.

By experimentally determining both the local degradation rates of the drug in the tissue and the toxic/therapeutic thresholds, an administration scheme can be formulated to describe how best to deliver the drug (either through a single delivery method, or repetitive dosing, which will slowly level out in such a way that the average delivery over time matches the local degradation rate at the desired concentration in the tissue).

Bioreactor Design

SPECIFICATIONS

The bioreactor system designed must accommodate perfusion flow at a constant flow rate, continuous media extraction/replenishment, no leakage, have an optical imaging interface compatible with an inverted confocal microscope with a working distance of less than 0.4 mm, and be capable of long term testing without contamination. The chamber should be capable of holding an engineered sample of human tissue flush and secure with the imaging interface to allow for easy imaging. These specifications are

highlighted in Table 5, along with some preliminary design features intended to meet these needs.

Required Need	Design Feature	Purpose
Sterility	-2 scaffolds/chamber design	-Prevents spread of contamination
	-Careful choice of materials with desired properties	-Autoclave-able, corrosion resistant, capable of being machined to a smooth finish
Imaging Compatibility	-Cover glass molded using PDMS to bottom of chambers	-Allows for secured viewing using inverted microscope
Functionality over weeks/ months	-Bioreactor chamber designed to be compatible with a Peristaltic Pump	-Allows slow, laminar, controlled flow rates over extended periods of time -Low chance of leakage
	-Bioreactor system held in sterile incubator at 37°C	-Tissues remain in *in vivo*-like temperature range

Table 5. Bioreactor system specifications along with the design features to be implemented to meet those specifications, and a description of each design features purpose and how they will satisfy the required need.

The bioreactor design will be considered successful if it is shown that the system can maintain a steady flow rate over weeks to months with minimal to no contamination or leakage. The most likely causes of a chamber failing to last throughout an experiment would be either contamination or leakage, which would be most likely to occur through a broken cover glass, loose connections with the tubing, or during media exchange. The goal is to have as many chambers survive the entire testing process without contamination.

CHAMBER

The design of a custom bioreactor began must include features allowing it to meet all the specifications labeled above, namely; sterility, cover glass imaging interface, perfusion inflow/outflow ports, and the ability of holding the tissue flush to the imaging interface.

Custom Design

The material to be used would need to be autoclave-able, machine-able, corrosion resistant, non-leaching, and mechanically rigid. It would also be ideal to use a transparent material for visual inspection throughout testing. To meet these goals, polycarbonate would be an ideal material because of its material properties meeting these specifications. If polycarbonate were found to be too difficult to machine, or was prone to cracking, then 316 Stainless steel would also meet all these specifications with the exception of transparency.

A prototype design for the custom built bioreactor chamber is shown in Figure 10. The chamber was designed to accommodate an 8x8x8mm cubic tissue held within 8x8mm square machined 7 mm into the center of the chamber. The reason for only a 7 mm depth in the mold to hold an 8 mm cubic is to hold the tissue face flush with the imaging interface for continuous monitoring throughout testing.

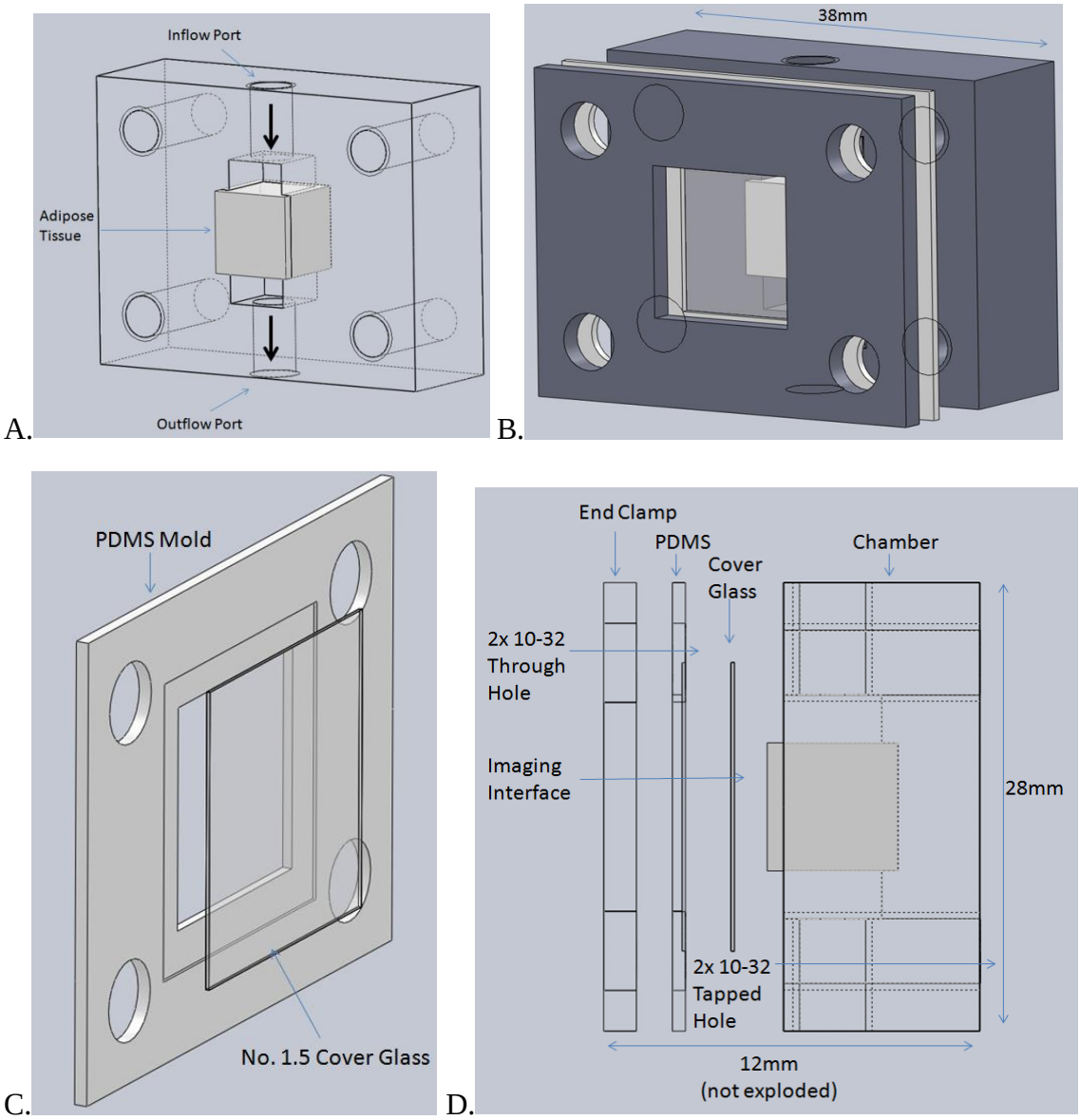

Figure 10. Preliminary design of a custom bioreactor chamber. A) Bioreactor chamber holding an 8x8x8mm cube of adipose tissue within a mold. B) Total configuration showing an opening through the polycarbonate end clamp with a cover glass imaging interface open to an objective. C) PDMS mold within which an 18x18mm square cover glass is set. The cover glass has a mold for it within the PDMS, but it will be fastened tight within the mold and polycarbonate chamber by tightening 4x10-32 screws at each corner. D) Exploded side view of chamber system showing its assembly. Note how the 8x8x8mm tissue protrudes from its mold (1mm). This is because the mold it is held in is only 7mm deep to keep the tissue slightly compressed in that dimension to hold it consistently flush with the imaging interface throughout testing.

The chamber would accommodate in/outflow ports to provide perfusion through the adipose tissue. These ports would be fastened with a polypropylene 10-32 UNF thread-classic series barb connector (ValuePlastics). Between the tissue and the in/outflow ports is a machined transition space that ensures that the perfusing medium spreads throughout the entirety of the tissue and isn't localized to a stream of diameter equal to the 10-32 inflow port. This design optimization was implemented to ensure that perfusion occurs throughout the tissue, particularly at the imaging interface (Figure 10A).

The cover glass is held flush with the bioreactor chamber and tissue construct from its position in a PDMS mold (Figure 10C). This has been shown to be a successful technique for holding a cover glass stationery and flush with a tissue, while also serving as a gasket between two rigid surfaces to prevent contamination and leakage (Kluge et al., 2011). The PDMS mold accommodates the 18x18mm dimensions of a square No. 1.5 cover glass with a 0.20 mm depression to accommodate the cover glass thickness.

The bioreactor chamber/tissue/cover glass/PDMS mold system will be held enclosed by fastening an end clamp through each construct via 4x10-32 threaded fasteners (Figure 10D). This should be sufficient to not only secure all pieces of the system together, but also ensure that the tissue/media system remains a closed system with respect to its environment. The thickness of the PDMS mold and clamping mechanism can be altered to accommodate the dimensions of the objective being used to ensure that the objective can come within close enough contact with the cover glass imaging interface to accommodate optimal penetration depth when imaging the tissue *in situ*.

Commercial System

A bioreactor chamber similar to the one needed for this project (3DKUBE™) was released by Kiyatec, 2011. The chamber accommodates a segregated culture of two samples and is compatible with unidirectional perfusion flow with imaging interface (Figure 11A). The 3DKUBE™ independent chamber configuration has been shown to be capable of *in situ* histological embedding, determining cell viability *in situ* via bioluminescence, and low magnification confocal microscopy (Figure 11B) (White, et al 2011).

A. 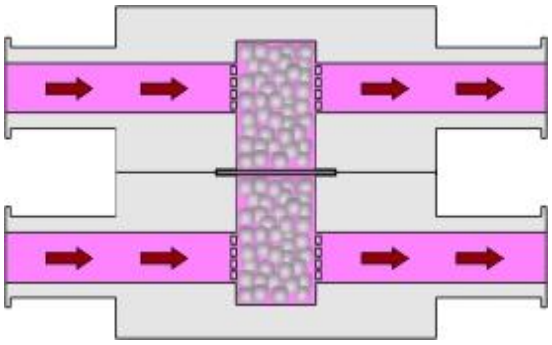 B. 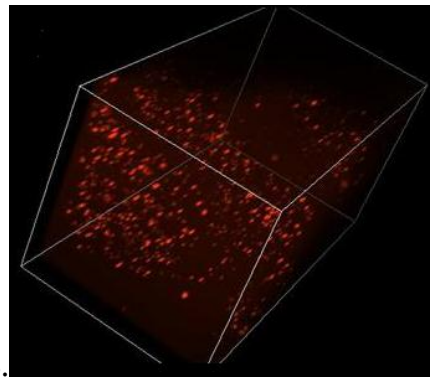

Figure 11. A) Flow profile of a 2 chamber Kiyatec 3DKUBE™ with independent chambers (no cross talk between upper and lower chambers). The inner diameter of the chambers is 6mm with an 8.8mm height. Media flow is unidirectional through inflow and outflow female luer lock connector ports. B) Laser confocal microscopy image of viable HepG2 cells stained with red fluorescent dye cultured encapsulated in alginate beads at 100x total magnification from within the 3DKUBE™ (White 2011).

Imaging Interface

However, the imaging interface of the 3DKUBE™ as bought is a 1.25mm thick polystyrene plastic (Figure 12A). Both the thickness and material properties of this

imaging interface are inappropriate for the high magnification multi photon imaging modalities desired for this project (outlined in specifications).

To accommodate TPEF imaging at a 63x objective the 3DKUBE™ polystyrene imaging interface would need to be bored out of the 3DKUBE™ chamber using a 15/48" diameter drill bit on a milling machine. To replace the polystyrene plastic, a No.1.5 thickness Fischer Scientific cover glass would be adhered over the new hole in the chamber as a replacement imaging interface (Figure 12B). This thickness allows for a 200µm penetration depth using the 63x objective available. This cover glass and thickness has been used in previous work for the same multi photon analyses looking to be performed here (Quinn et al., 2011).

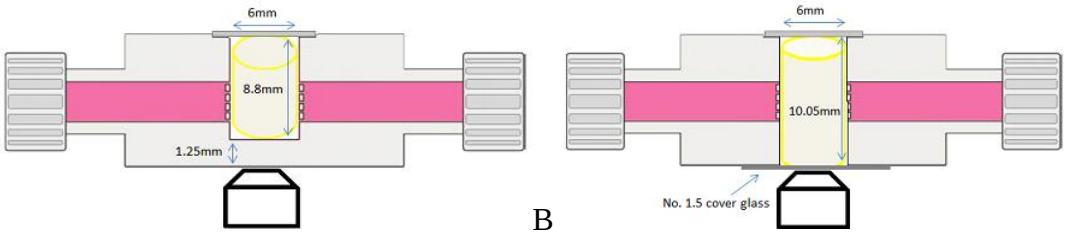

A. B

Figure 12. A.) Scaffold/3DKUBE™ dimensions as bought provides for a 1.25mm thick polystyrene imaging window for any objective. B.) After boring out the polystyrene plastic a larger scaffold can be input to the chamber to hold the tissue flush with a No. 1.5 (200µm) thick cover glass affording a 200µm penetration depth into the tissue using a 63x objective.

After experimenting with multiple adhesive strategies, Loctite 4541 was found to be an appropriate adhesive to bond the cover glass to the 3DKUBE™ chamber. This decision was based on its adhesive capabilities, biocompatibility, and ability to withstand various sterilization techniques. Loctite 4541 is ISO 10993 compliant, which is an evaluation standard used for chemicals coming in contact with biological tissues in medical devices.

It is also capable of maintaining its adhesive properties through both EtO and autoclave sterilization cycles. It was designed specifically for materials that are difficult for other glues to adhere to (i.e. plastics and metals).

CUSTOM VS. 3DKUBE™

The strengths and weaknesses of the 3DKUBE™ and custom designed chambers are shown in Table 6. After reviewing and comparing the two options, and because of the preliminary nature of this work, the cost advantage of using the 3DKUBE™ chamber was the deciding factor in choosing which design to pursue. The 3DKUBE™ has also comes with proven functionality and provides a great ease of use with regards to the system setup. Therefore, the research outlined in this thesis was continued using the commercially bought Kiyatec 3DKUBE™ with the aforementioned modifications.

MEDIA RESERVOIR

Considering the small volume within the 3DKUBE™ chamber (6x8.8mm, dxh), an external media reservoir is required to sustain the 3D tissue. For this purpose, the barrel of a 30mL syringe with the plunger removed was used (Figure 13A). The open top of the syringe was then plugged shut using a Size 3 VWR Black Rubber Stopper. The inner diameter of a 30mL syringe is roughly 21.7 mm. A Size 3 rubber stopper is 25 mm long with an upper diameter of 24 mm and a lower diameter of 18mm, allowing it to be press fit into the top of the syringe, providing an air tight seal.

Specification	3DKUBE	Custom Design
Sterility	One experienced contamination	All autoclave-able parts
Setup	Easy construction and one piece design saves time	Many different pieces and machined parts complicate setup
Imaging Interface	Demonstrated to not break/fracture during imaging when contacted by objective	Site of tissue surface flush with imaging interface is more representative of tissue section subjected to perfusion flow
Functionality over weeks/ months	Up to 5wks perfusion observed Vulnerable to leaks at custom imaging interface	Proven gasket design to **prevent leaks while maintaining** cover glass flush with system Option to use adhesive in supplement to gasket
Tissue Orientation	Tissues housed in opposite orientation	All tissues oriented on one side of chamber for improved assurance media flows through tissue at site of imaging interface
Cost	Considerably cheaper ($220/box)	Higher PDMS/Polycarbonate/Machining costs

Table 6. Side by side comparison of the strengths and weaknesses of the 3DKUBE™ chamber and custom designed chamber.

GAS EXCHANGE

In order to supply oxygen and remove carbon dioxide from the tissue/chamber system, an outlet for gas exchange must be present. For this purpose, a Millex-FG, 0.22µm, hydrophobic PTFE, 25 mm diameter, EtO sterilized air filter was used. The gas exchange port was put at the site of the black rubber stopper at the top of the media reservoir (Figure 13A). To reach through the stopper, a 16 gauge 1.5" needle was used to puncture through the 25mm long rubber stopper. A male luer lock to barb connection was connected to the needle's complimentary female luer lock connection. From the barb, a 1-2" strand of Silicon Platinum cured tubing (ID 1/16") was used to connect the needle-barb connection to the female luer lock connector of the air filter through another barb to

male luer lock connection. This provided for a source of sterile gas exchange above the surface of the media within the media reservoir.

A.  B.  C. 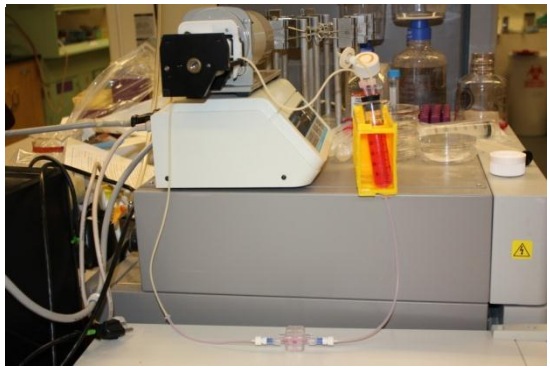

Figure 13. A. Configuration of media reservoir made up of a 30mL syringe barrel with a rubber stopper plugging up its open two. The two syringes piercing through the rubber stopper are connected to two male luer lock to barb connections which connect to tubes that lead out to a gas exchange and media flow in port. The female barb on the bottom of the syringe leads to the bioreactor chamber (Note; during testing/imaging phenol red free media was used). B. 3DKUBE™ chamber with polystyrene bored out and cover glass glued on using Loctite adhesive (gray ring around imaging interface). C. Perfusion flow circuit showing entire configuration from chamber to pump to media reservoir plus connections.

FLOW CIRCUIT

The three main components of this perfusion bioreactor system are the chamber, peristaltic pump, and media reservoir/gas exchange. These three components are all connected in series as shown in Figure 13C via platinum cured silicone and PharMed tubing (Cole Parmer, Vernon Hills, IL) and luer lock to barb connections. With the orientation shown in Figure 13C, the media flows in the clockwise direction so that

media drops into the 30mL syringe media reservoir (rather than being sucked up through the top). This keeps the gas exchange (shown adjacent to media inflow port in Figure 13A) dry and prevents contamination.

FLOW RATE

The flow rate of the perfusion pumping mechanism could be controlled by two parameters; the rotations per minute of the peristaltic pump and the inner diameter of the PharMed tubing that the pump was operating on. The practice of tissue engineering is delicate during the early stages of tissue growth because of the low density of cells that often adhere to the scaffold material. There is also no ECM growth at the start of tissue culture and so the cells must begin by generating their own within the pores of the scaffold. Given this delicate nature, slower flow rates were preferred, and as mentioned earlier, optimal flow rates for other tissue engineering applications have been found to be on the order of 400-800 μm/s (Grayson et al., 2011).

The minimum rotations per minute permitted by the pumping mechanism used were 10rpm. From there, the inner diameter of the PharMed tubing could be controlled to tailor the flow rates to the desired levels. Masterflex PharMed tubing size #13 has an inner diameter of 0.03". After measuring the flow rates multiple times (n=3) and averaging the measurements, an average flow rate of 0.0056875 mL/s was measured. By taking into account the cross sectional area of the bioreactor chamber in/outflow ports, the lateral flow rate perfusing through the adipose tissue samples within the bioreactor chambers was calculated to be 412.5 μm/s. This is the flow rate that was used throughout the

experiments to be described. It can be altered for future experiments by either changing the speed of the motor, or by using tubing with a different inner diameter.

STERILITY

As mentioned in the specifications, each and every part of the perfusion bioreactor system that encloses or comes in direct contact with the internal tissue/media reservoir system must be sterilized. The tissue/media reservoir system should also be completely closed off from any sources of contamination from the bioreactor surroundings.

The two modes of sterilization utilized in the design of this perfusion bioreactor system are autoclave and EtO sterilization. Autoclave was considered the preferred method, and so as many bioreactor components as possible were chosen from autoclave-able materials. All of the connectors (barb to barb, male/female luer lock to barb) were made of autoclave-able propylene. Both types of tubing (PharMed, platinum cured silicone) were autoclave-able, along with the Loctite adhesive after being allowed to dry. The syringe used for the media reservoir and the 3DKUBE™ chambers however were made out of non-autoclave-able plastics. Because of this, they were both sterilized through EtO sterilization. All syringe needles and air filters used here were purchased after having already been EtO sterilized.

To ensure that the tissue/media reservoir system remained closed to the outside environment throughout testing, the same Loctite adhesive used to connect the cover glass to the 3DKUBE™ chamber was generously applied around each and every tube-tube, tube-chamber, tube-syringe, tube-needle, tube-filter, needle-rubber stopper, and rubber stopper-syringe connection in the perfusion flow circuit. Each of these

connections as is are already supposed to be air tight and unlikely sources of contamination as advertised, but considering the number of connections (and possible sources of contamination), it was considered worthwhile to alleviate any unnecessary risk and generously apply the highly viscous Loctite adhesive to each of these connections for added security from sources of contamination.

PERFORMANCE MEASURED

The goal of this design was to build a perfusion bioreactor system that would allow for noninvasive, continuous analysis of adipose tissue samples via confocal multi photon microscopy, media extraction, and eventual destructive histological analysis (Figure 14). The focus of the results displayed in the perfusion bioreactor experimental section was on a three week experiment where the adipose tissue samples were held in perfusion flow within the outlined bioreactor system for the last two weeks of the experiment. Eleven tissues in total were placed within the perfusion bioreactor system where multiple samples were imaged and sacrificed for histological analysis at the 0wk, 1wk, and 2wk time points. The measure of how the bioreactor system performed throughout this experiment is shown below in Table 6, and also described here.

Of the eleven samples introduced to the system, only three failed to last until their scheduled sacrificial time point. Two of those samples failed as a result of a leak at the site of the imaging interface where the cover glass had been glued onto the 3DKUBE™. The other was a result of contamination.

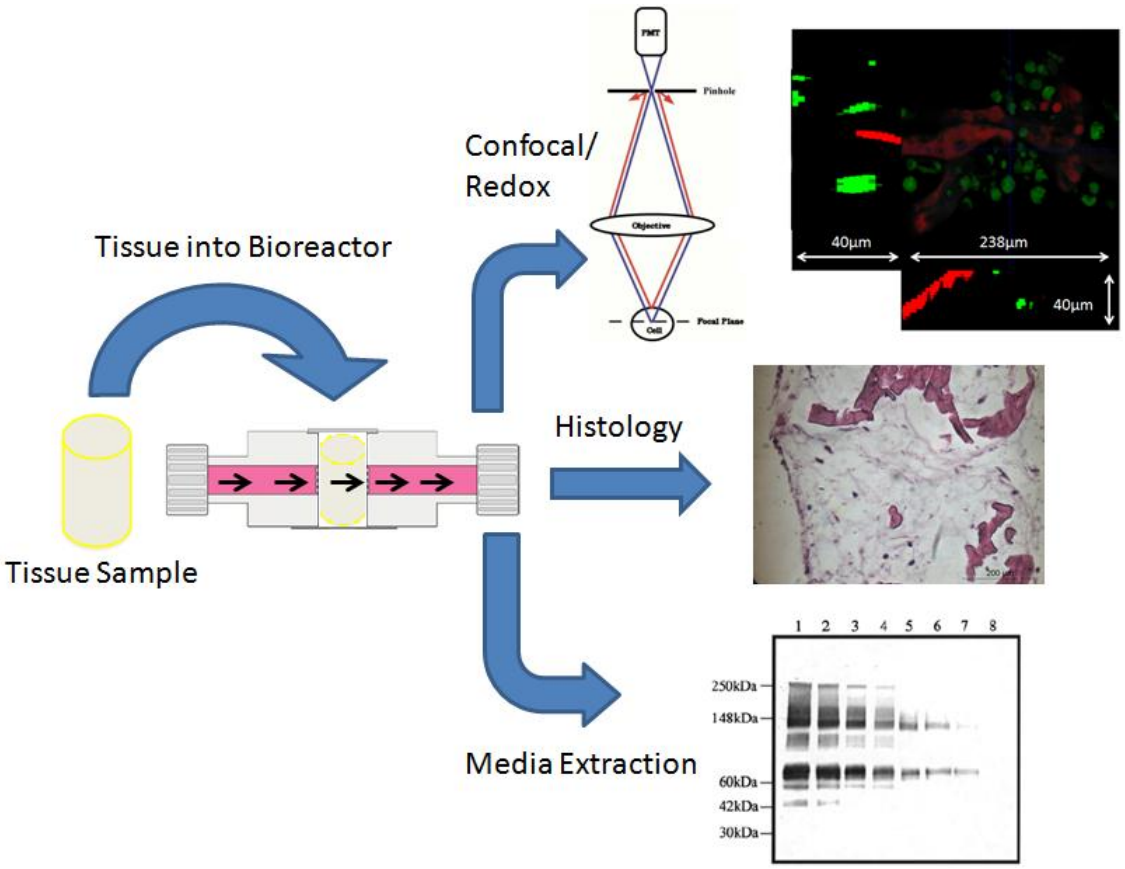

Figure 14. Schematic showing the path of the tissue from static culture into the perfusion environment of the bioreactor chamber, and then the three modes of analysis afforded through this bioreactor system. The confocal image shows the silk and cells false colored red and green, respectively, with two cross sectional images, showing the depth resolved 40 µm image stack, displayed on the left and bottom of the image (cross sections taken through the center of the image). Histology shows an H&E stained adipose tissue sample. Media extraction allows for analysis of the perfusing medium and any biomolecules excreted from the cells into it through assays or western blot analysis (Hughes, et al 2003)

In the two cases where testing was ended as a result of a leak, extra media was added to the media reservoir to test to see if the bioreactor system was capable of sterile media exchange and replenishment. In both these cases, the bioreactor systems were allowed to continue to run on replenished media reserves, and in both cases, the samples were able to run with media for another day (and then again, for a second day after another media

replenishment) without contamination before the replenished media had leaked out again. This observation implies two things. First, that the leak in the chamber appears to be large enough for media to leak out of, but small enough to prevent the entrance of any contamination. Second, the bioreactor system is capable of sterile media exchange and replenishment during testing. This is important with regards to future applications of the bioreactor system including but not limited to drug testing, where protein excretion from the tissue can be used to assess metabolic activities.

Two samples were able to reach the 2wk time point. Since then, another sample (which was not analyzed, but only used to measure the longevity of the bioreactor functionality without contamination or leakage) has lasted up to 5wks in culture within the bioreactor. This shows that for now, the bioreactor system has demonstrated the capability of sterile functionality for at least two, and likely for more weeks. The samples that lasted to the 2wk time point were chosen to be sacrificed to obtain samples for histological analysis to compare to previous 3wk studies, and by no means were sacrificed as a result of any problem with the functional perfusion or sterility of the system.

At the 0wk, 1wk, and 2wk time points, the adipose tissue samples within the 3DKUBE™ were imaged *in situ* using TPEF imaging with both a 20x and 63x objective. The data obtained from the subsequent redox ratio analysis will be described later, but the ability of the bioreactor chambers to allow for real time imaging before, during, and after an experiment where it was exposed to perfusion flow is considered a success. At each imaging time point, the particular chamber to be imaged was removed (with its media reservoir) from the peristaltic pump and secured onto the imaging stand of an inverted confocal microscope. Throughout testing, there was no instance where the objective

broke the cover glass at the imaging interface, and there was never a leak or break during imaging. There was never a sample held flush with the imaging interface that was not able to be imaged.

Specification	Performance	Grade
Sterility	-8 out of 11 samples remained sterile from the time they were introduced to the bioreactor to the time they were scheduled for removal (two leaks, one contamination)	++
Imaging Compatibility	-All tissues were able to be successfully imaged using a 63x objective inverted microscope giving a 200um penetration depth -No elements of the bioreactor system were damaged during the process of imaging -Images acquired were of sufficient quality for redox ratio analysis	+++
Functionality over weeks/ months	-Two samples were successfully maintained within system under laminar perfusion flow and without contamination for 5wks	++
Flow Rate	-412.5 μm/s later flow rate achieved on tissues in bioreactor chamber with capabilities of increasing/decreasing this rate	+++

Table 7. Evaluation of how the perfusion bioreactor system met the specifications outlined before. Grade scale: Minus sign implies a failure. A success is graded from one to three '+'s.

The flow rate achieved and used throughout this experiment was 412.5μm/s. Previous research shows that optimal flow rates for tissue engineering purposes are 400-800 μm/s (Grayson et al., 2011). It is at these later flow rates that cells can be cultured on 3D scaffolds without being washed off of the scaffolds (as would happen with too high of flow rates), but the cells are still mechanically encouraged to homogenously spread throughout the inner porous spaces within the scaffold, and nutrients can be adequately

spread within these spaces through sufficient perfusion flow. Our flow rates are able to be increased or decreased still by altering the rotation speed of the motor and the inner diameter of the tubing. This was considered a success with regards to the desired flow rates and customizability that future experiments may require of the system.

Tissue Engineering

In order to test the effects of novel drug delivery on engineered 3D human tissue with the aims of actually improving the efficiency with which human biological systems are modeled and analyzed *in vitro*, it is necessary to choose a 3D tissue model that is both clinically relevant and has been proven to accurately represent a viable and realistic model of native human tissue.

To be clinically relevant, the tissue should be the host of serious pathophysiolological disorders. These include but of course are not limited to various cancers, chronic/acute inflammation, mechanical weakening (i.e., the cervix), diabetes, obesity, sexually transmitted diseases, etc. The tissue should also be the direct target of both clinically approved and experimental molecular entities of drugs so as to ensure its relevance in eventually using the system as a possible drug screening platform. .

Just as important as the clinical relevance of the tissue, is the proof corresponding to the validation of the engineered tissue as a viable and appropriate model for its native human counterpart. This could require extensive biochemical, electrical, mechanical, and imaging analysis of the engineered 3D tissue model. Vascularization will also be considered of paramount importance so that any drugs delivered to the tissue system will

be able to permeate through the entirety of the construct, mimicking the actual scenario of drug delivery to native tissue *in vivo*.

ADIPOSE TISSUE

Human white adipose tissue was selected for study due to the wide range of disorders associated with this tissue (diabetes, metabolic diseases, and obesity) and their overall growing impact on human health. Obesity alone is considered to account for 4.32% of all healthcare costs in the US for citizens between the ages of 20-85yrs, and the average medical expenditures incurred by diabetics in the US averages to be about 2.4 times that of individuals without diabetes (American Diabetes Association 2003; Allison et al., 1999). Further, we have extensive experience in growing 3D human adipose tissues and studying these systems both in vitro and in vivo (Mauney et al., 2007; Kang et al., 2009; Choi et al., 2010), providing a solid foundation for the current plans.

Engineered 3D Human Vascularized Adipose Tissue

As mentioned before, the protocols for engineering 3D vascularized human adipose tissue have been described before (Kang et al., 2009). In short, both human adipose derived stem cells (hASCs) and human umbilical vein endothelial cells (HUVECs) are grown to confluency in their own respective 2D cultures before being seeded onto porous silk scaffolds at specific cell densities at specific time points (Table 7).

Cell Type	Differentiation/Growth Media	Seeding Day	Cells/Scaffold
hASCs	DMEM/F-12 supplemented with 10% FBS and 1% antibiotic–antimycotic	7	400,000
HUVECs	Endothelial Growth Medium	0	800,000

Table 8. Vascularized 3D Adipose tissue engineering protocols using human umbilical vein endothelial cells (HUVECs) and human adipose derived stem cells (hASCs). After 7 days differentiation, hASCs are added to HUVEC seeded scaffolds in a 1:1 ratio of Endothelial Growth Medium and Adipocyte Maintenance Medium. At Day 21, tissue will be ready for testing.

Silk Scaffolds

We have previously described in detail the preparation and characterization of porous silk scaffolds for the system. The logic for this material is the mechanical durability and very slow degradation (months to years), along with biocompatibility and success in 3D adipose tissue formation in our prior studies (Kang et al., 2009; Quinn et al., 2011). The silk used was extracted from the cocoons of the Bombyx mori silkworm, mixed with a 0.2M sodium carbonate solution, boiled and rinsed repeatedly in distilled water, and then dissolved in a 9.3M lithium bromide solution. The resulting lithium and bromide ions were then removed through a series of dialysis against distilled water before being centrifuged to remove any particulates. An 8% w/v silk concentration was used, to which 4 g of sieved granular sodium chloride, of particle sizes 500-600 microns, was added to 2mL silk solution and allowed to solidify for 72 hrs at room temperature. The scaffolds that formed were rinsed in distilled water for 48 hrs while the salt particles leached out. The final scaffolds were punched out into 8x4mm (dxh) scaffolds. The scaffolds were autoclaved for sterilization prior to cell seeding.

Cell Seeding

All protocols will follow our prior publications (Kang et al., 2009). The scaffolds will be soaked in medium for 24 hrs in an incubator and then the HUVECs will be seeded at 800,000 cells/scaffold and hASCs will be placed into adipocyte induction media. Seven days later, the differentiated adipocytes will be seeded onto the same scaffolds at 375,000 cells/scaffold. The media will be a 1:1 ratio of endothelial growth medium to both hASC growth medium and differentiated adipocyte medium (minus IBMX and TZD). The constructs will remain in a static environment during incubation for 21 days to allow for vascularized 3D adipose tissue to form.

STATIC ANALYSIS

Before introducing the 3D human tissue engineered adipose samples to the perfusion bioreactor system, it was first necessary to make sure that the static culture tissue samples were cultured successfully to ensure that the previously described protocols were correctly followed. The tissues samples were analyzed through both destructive histological methods and noninvasive imaging techniques.

An appropriate histological stain often used to assess the growth state of adipose tissue is through hematoxylin and eosin staining (H&E staining). To compare the confluency of cell and tissue growth within the silk scaffolds as a function of time, tissues were sacrificed for H&E staining and redox ratio analysis at both 3 and 10wks post HUVEC

seeding. It should be noted, that according to the protocols put forth by Kang et al., 2009, these adipose tissue samples are considered mature 3wks post HUVEC seeding.

Results

H&E

Images were taken using both 20x and 40x objectives of tissues at 3wks and 10wks maturity. To understand the cell/ECM density behavior as a function of depth, both the outer edges and middle regions of the tissues were observed separately (Figures 15 and 16, respectively). The outer edges are clearly observed in Figure 15 to be the edge of the tissue as observed under the specified magnifications. The edge being shown is the bottom of the tissue which is to be imaged through redox ratio analysis later. The middle region being imaged in Figure 16 was taken from slicing the cylinder shaped tissues down the middle to make two hemi-cylinders. The rectangular face resulting from slicing into the new face of the hemi cylinder was then imaged in the exact center to give a representative image of the innermost tissue space from within the tissue.

Within these images, the thick dark purple structures are the silk scaffold. The lighter purple elongated structures are cells, and within them there are easily discerned dark spots which are the cellular nuclei. The packets of cells enclosed within the dark purple silk structures are the silk pores made from the salt crystals during silk scaffold production. By comparing the size of these pores in the 20x objective images to their respective scale bars, it can be observed that the pores are in fact on the order of 500-

600µm in diameter, which makes sense because that is the size of the salt crystals described earlier in the silk protocols.

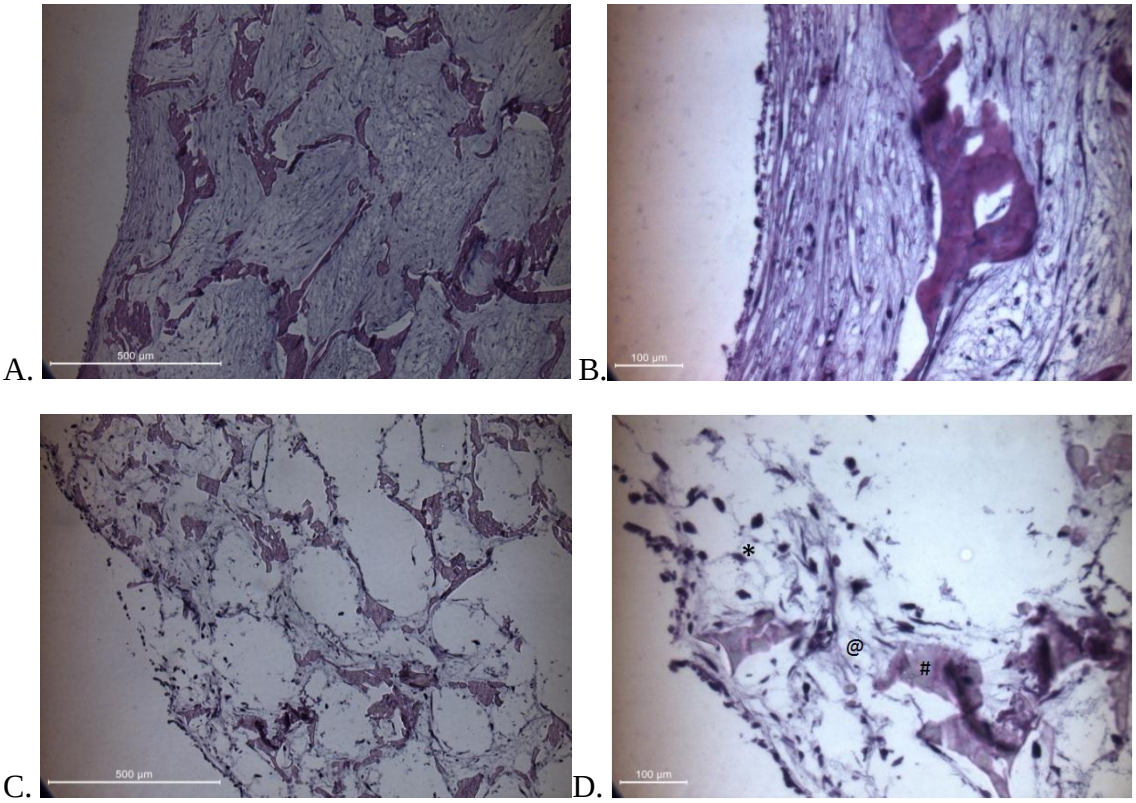

Figure 15. H&E stained histology images of adipose tissue grown in static culture within a multi-well plate. Each image is taken from the edge of the histological sample associated with the bottom of the tissue which will be imaged during the redox ratio analysis later. A) 10wks at 20x objective. B) 10wks at 40x objective. C) 3wks at 20x objective. D) 3wks at 40x objective. Within each image, the large dark purple structures are the silk scaffold (labeled '#' in D). The lighter colored purple that is sparsely formed between the silk scaffolds is ECM (labeled '@' in D). The sparsely distributed dark black objects are cells/cell nuclei (labeled '*' in D).

As is observed in Figures 15 and 16, the cell and overall cellularity and ECM growth are considerably greater in the more mature 10wk tissues than 3wk. This shows that although the tissues have been shown to be viable adipose tissue samples after 3wks (Kang et al.,

2009), tissue growth will continue within the pores of the silk scaffolds, as is shown in the 10wk images.

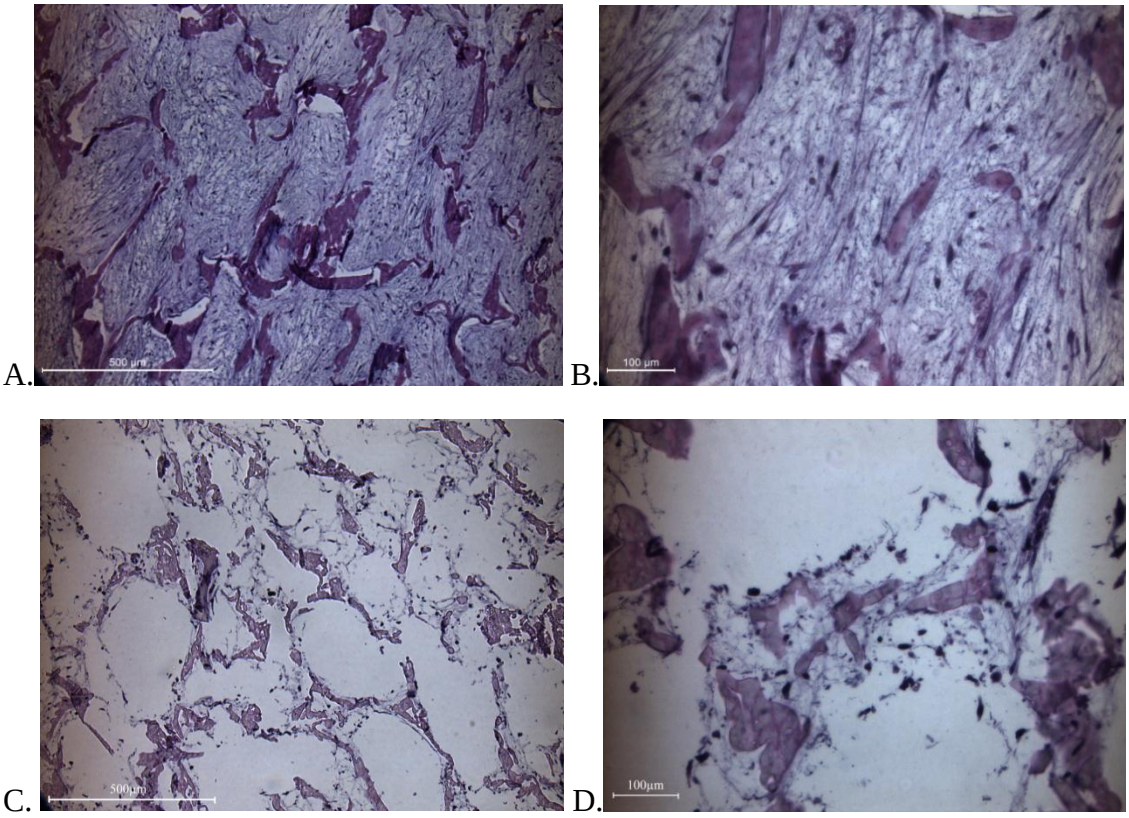

Figure 16. H&E stained histology images of adipose tissue grown in static culture within a multi-well plate. Each image is taken from the center of mass of the adipose tissue samples. A) 10wks at 20x objective. B) 10wks at 40x objective. C) 3wks at 20x objective. D) 3wks at 40x objective.

In comparing the images of Figures 15 and 16, it can also be observed that with regards to the 3wk time point, the silk scaffolds are considerably denser with tissue growth and cell density along the outer edge of the scaffolds. Deeper into the tissues (Figure 16) have more open space and less cells. This is a trend that has been observed in other histological and imaging work performed on engineered adipose tissue constructs similar

to these (Quinn et al., 2011). This represents a depth dependence on tissue growth rates on these silk scaffolds, and will come up again during the imaging measurements later.

Noninvasive Analysis

The aim of this work is to noninvasively characterize metabolic changes in adipose tissue through solely endogenous fluorophores as a function of tissue maturity. The data in this section was gathered in static culture from samples cultured in multi-well plates. The available technologies capable of accomplishing these goals are fluorescence and subsequent image processing (redox ratio analysis). Redox ratio analysis provides information into the metabolic activity of cells, and as used in this research, redox ratio analysis relies entirely on endogenous fluorophores as sources of contrast.

Before introducing the tissue samples to the bioreactor system, preliminary redox ratio analysis was performed on static culture tissue samples to correlate with the previously described H&E stained samples taken at 3wks and 10wks, and also to previous work performed on the analysis of tissue engineered 3D human adipose tissue in static culture using redox ratio analysis (Quinn et al., 2011). The aim is to noninvasively obtain information on the metabolic/morphological changes in the tissue including but not limited to cell size, ECM degradation, tissue genesis, cell proliferation, cell differentiation, cell shape, and expression of specific metabolic intermediates. This allows for two different analyses of engineered adipose tissue and offers the opportunity to ensure that the 3D vascularized adipose tissue engineering protocols are being

correctly executed while also being able to compare the data obtained through the stains and redox ratio analysis to better support any conclusions made.

PROTOCOL

After culturing adipose tissue samples in static culture from within multi-well plates for 3 and 10 wks, they were analyzed for redox ratio analysis. Adipose tissue samples were excited using a two photon fluorescence system using a Ti:Sapphire tunable laser. TPEF imaging was appropriate because it allowed for up to 200μm imaging depths within the tissues while also limiting photo damage to the tissues.

The redox ratio calculated (FAD/(NADH+FAD)) has been used extensively throughout the literature to measure metabolic activity (Rice et al., 2007; Quinn et al., 2011). The protocols followed in this particular work follow those put forth by Quinn et al, 2011.

Adipose tissue samples were held flush with an imaging interface that was a No. 1.5 thickness cover glass to allow for 200μm penetration depth using a 63x objective on a confocal microscope. Fluorophore excitation was provided with a tunable Ti:Sapphire laser (Mai Tai; Spectra Physics; Mountain View, CA). Images were taken using a Leica TCS SPC2 confocal microscope with a water immersion 63x objective.

In accordance with the ex/em wavelengths of NAD(P)H and FAD shown earlier in Figure 5, samples were excited at 755nm and 860nm, and the corresponding emission spectra of the target fluorophores were gathered at 460(±20)nm (NAD(P)H) and a 525(±25)nm (FAD).

Given a penetration depth of 200µm into the tissue, a series of depth resolved images were taken from 0-40µm, 80-120µm, and 160-200µm at 2.5µm increments. Each of these series was then run through a custom image processing program in MatLab that utilized a linear discriminant analysis to distinguish between cells and the external environment (i.e., blank space and scaffold structure) by differentiating cells on the basis of shape and fluorescent intensities.

After identifying the cells within the 3D depth resolved images, the program performs an analysis on the shape, volume, biochemical concentration (NAD(P)H, FAD, Lipofuscin) and redox state of the imaged cell populations. The redox state of each cell being calculated through a series of scalar intensity analyses. The fluorescence intensity at each ex/em combination was normalized from its 12-bit intensity reading. The ex/em combinations that characterize the presence of NAD(P)H and FAD were converted to scalar values to allow for the simple redox ratio arithmetic to obtain relative redox ratio values for each pixel of the acquired images. From here, the redox state of each cell could be expressed using a false color redox map.

RESULTS

After verifying that the adipose tissue samples grown at 3wks and 10wks maturity (post-HUVEC seeding) were viable through H&E staining, the tissues were analyzed through redox ratio analysis. As shown through H&E, the cell density showed a considerable increase with greater maturity (more cells found in 10wk coculture than in 3wk coculture), as shown in Figure 17A and 17C. However, the redox ratios of each cell did

not show a significant difference between the two groups (Figure 6a and 6b). This is not an unlikely outcome considering that neither of the tissues was treated with any particular treatment that the other wasn't. Instead, the primary cellular/tissue differences that should be significant are cell density. The increase in cell density is supported by our previous H&E stains and Quinn et al., 2011.

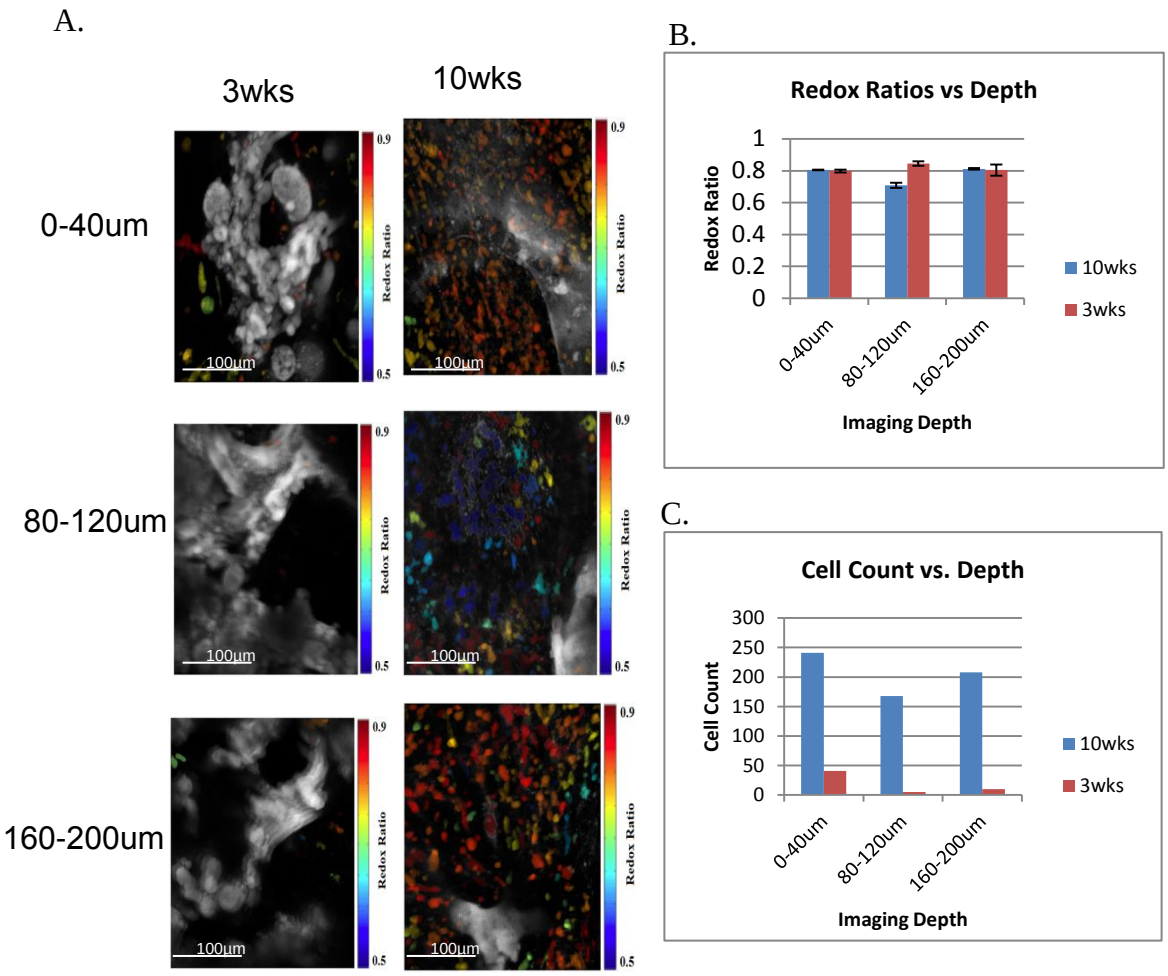

Figure 17. Redox ratio and cellularity data from adipose tissue samples cultured in static environment in multi-well plates. A) False color redox ratio maps of adipose tissues grown in static culture for 10 and 3wks. B) Redox ratio vs depth for the tissues imaged in A. C) Cell count vs depth for tissues imaged in A.

With respect to the cell localization, it was shown in the previous H&E stains that more cells were located about the superficial, or surface layer of the tissues at 3wks, but that at 10wks the cells had spread throughout the entirety of the tissue. This is again supported through the imaging analysis (Figure 17C) where there is not a significant difference in cell density between each of the three imaged layers in the 10wk sample, but there is a significant decrease in cell population found as the penetration depth goes deeper and deeper into the tissue.

ADIPOSE TISSUE MATURITY EXPERIMENT

After establishing a successful perfusion bioreactor design, 3D human adipose tissue engineering protocols, and static redox ratio imaging analysis, all three components were combined to perform an experiment analyzing the metabolism of adipose tissue as it matures under a perfusion flow environment. The purpose of this experiment was to understand how perfusion can affect the metabolic activity of the tissue and to present a proof of concept for a perfusion bioreactor system w/imaging interface as a functional mode of real time metabolic analysis for 3D tissue constructs. The experiment was chosen to last for a total of 23 days in an attempt to emulate the timeline and protocols set forth by Kang et al., 2009, where adipose samples were analyzed for 21 days to assess functionality and first demonstrate the appropriateness of the adipose tissue used in this work as a representative model for native human adipose tissue. The histological, imaging, and redox ratio data obtained during the experiment could then be compared to

the results found by Kang et al., 2009, and Quinn et al., 2011, in their static cultures, and provide a basis for comparison for perfusion vs. static culture.

TIMELINE

The timeline put forth by Kang et al., 2009, that is being emulated in the design of this experiment was described before (Table 7), with the timeline for this experiment shown below in Figure 18. Because the tissues in this experiment are introduced to perfusion flow, cell adhesion to the silk scaffold is especially important. To accommodate this, the tissues were not introduced to the perfusion bioreactor system until day 9 (two days post-adipocyte seeding). The purpose of this is to ensure that all the adipocytes aren't brushed off the scaffold immediately after seeding by allowing for two days of adipocyte cell adhesion in static culture.

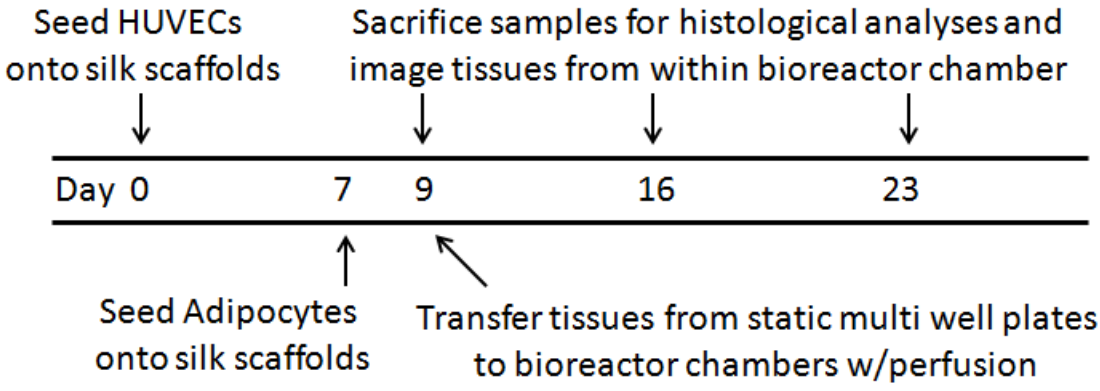

Figure 18. Timeline of the experiment described here. Notice that this is identical to the 3wk experimental timeline put forth by Kang et al., 2009, with the exception of the two days after day 7 which are included to allow ample time for the adipocytes to adhere to the silk scaffold prior to introducing the tissues to perfusion flow.

On days 9, 16, and 23, the samples were all imaged from within the 3DKUBE™ chamber through the custom fitted cover glass. In the data displayed later, days 9, 16, and 23 correspond to the time points 0wk, 1wk, and 2wks respectively. This is to signify 0wk, 1wk, and 2wks time in a perfusion environment.

TISSUE FITTING

In order to ensure that the adipose tissue imaging from within the 3DKUBE™ chamber is able to reach a penetration depth of 200µm, the adipose tissue scaffold design had to be tailored to ensure that the tissue remains flush with the inside surface of the bioreactor chamber's imaging interface at all times. As shown earlier in Figure 12, the height within the chamber after the cover glass has been attached is 10.05mm. To ensure that the tissue remained flush with the bottom surface of the chamber, the scaffolds were made larger than the 8x4mm (dxh) dimensions described by Kang, et al. Scaffolds were tailored to fit tightly within the chamber with dimensions of 6x10.05mm (dxh), and the appropriate cell seeding densities for HUVECs and adipocytes were scaled up accordingly (Figure 19).

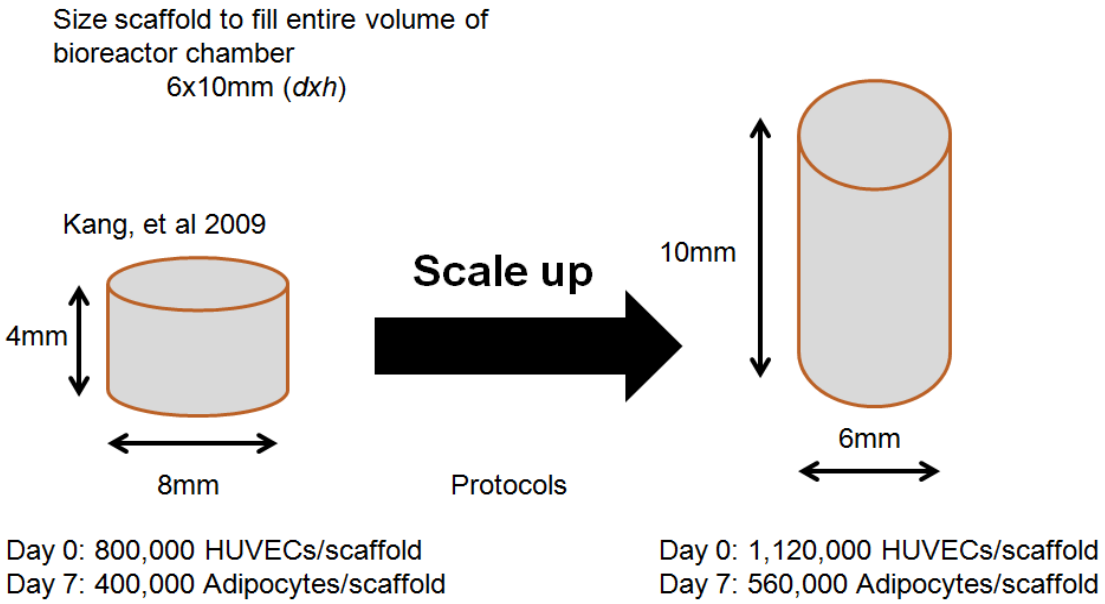

Figure 19. Scale up of dimensions and cell seeding densities to accommodate a larger scaffold/tissue size in order to fill entirely the inner space of the bioreactor chamber and hold the tissue flush with the inside imaging interface.

RESULTS

Imaging

As mentioned before, all of the images taken throughout the entirety of this experiment were taken with the adipose tissue samples being held within the bioreactor chamber, and images were taken through the cover glass interface. As seen in Figure 20, images were taken at three different depths and then run through the previously described Matlab program which identified the cells within the images and calculated redox ratios for each cell before displaying them in a false color map as shown. In the images shown, the white structures are the silk scaffold while the sporadically placed colored images are cells. Images are shown for the tissues after 0, 1, and 2wks in perfusion (1, 9, and 16 days post adipocyte seeding respectively). For comparison, the redox map of one of the tissues that

was held within one of the bioreactor chambers that ended up leaking out is included as well (2wk (dead)).

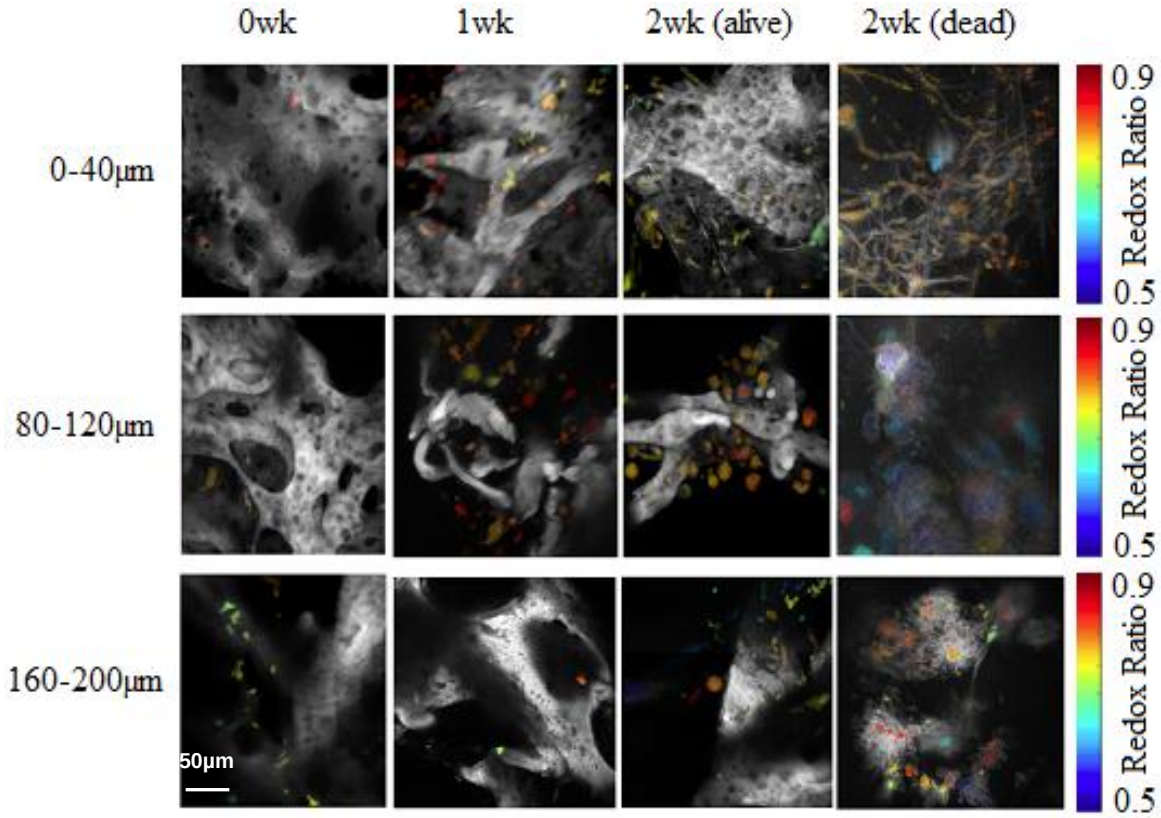

Figure 20. False colored Redox maps for adipose tissue images taken while within the bioreactor chambers after 0, 1, and 2wks within the perfusion environment. Images of one of the samples from within a chamber that leaked out are included to show contrast between live moist tissues and dead and dry tissues.

As was observed in the static cultures previously, the number of cells present in the images increases with time. This is in agreement with the findings of Quinn et al., 2011, performed in static culture as well. There is also an eventual aggregation of the cells within the superficial (0-40µm) range as time progresses from 0-1wks. This is in agreement with the previously shown static cell density conclusions drawn from cell

counting and H&E stains. At 0wks there does not appear to be a significantly larger cell density at the superficial layer compared to the deeper sections. This makes sense considering that the cells were only just seeded, and most likely did not have much opportunity to sift throughout the silk scaffold yet. However, at the time point of 2wks, the cellularity does appear to begin to level out within each of the layers (superficial, intermediate, and deep) in both the noninvasive imaging analysis and H&E stains. Longer experimental time points would be required to confirm this trend, but a more homogenous distribution of cells within a 3D scaffold in perfusion culture environment relative to static has been observed elsewhere (Grayson et al., 2011).

A. 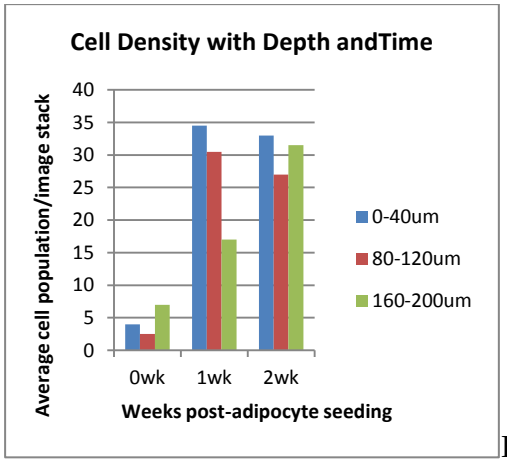

B. 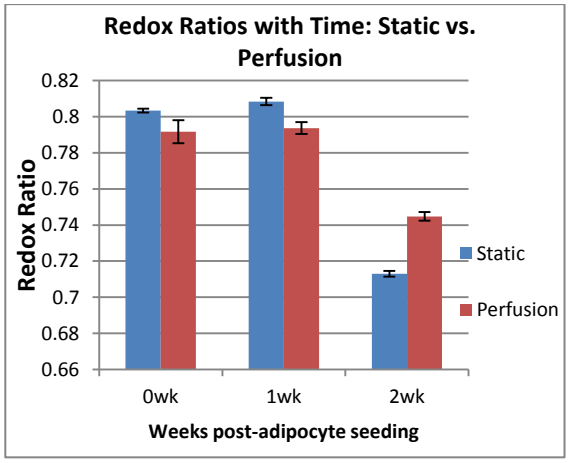

Figure 21. A) Cell population measurements made per 40µm image stack at 0, 1, and 2wks in perfusion flow. B) Average redox ratios at 0, 1, and 2wks in perfusion verses static culture. In both static and perfusion culture, comparing means showed with $p<0.05$ that the decrease in redox ratios from 1 to 2wks but not 0 to 1wk was significant. The difference in mean redox ratios was significant at at least $p<0.01$ between static and perfusion cultures at each time point.

This conclusion is supported in Figure 21A. At time point 0wk, there is not much of a trend when observing the cell densities with respect to depth within the tissue. However, what is apparent is that after 0wks, the cell populations do generally increase in all three image stack depths. This is a sign of continued cellular proliferation and distribution throughout the silk scaffolds. This again, is consistent with the previously described static cultures, and the static cultures analyzed by Quinn et al., 2011. It should be mentioned however that although it does appear that there tends to be a higher cell density at the superficial layer of the tissues, the trend is not significant at $p<0.05$.

After redox ratio calculations were performed on the images acquired, the data obtained from this perfusion system was compared side by side with data acquired from the static culture experiment by Quinn et al., 2011 for the time points of 0, 1, and 2wks. Although the average redox ratios for the perfusion and static cultures were not identical with one another throughout the first week (static culture: 0.80, perfusion culture: 0.79), neither culture showed a significant change in redox ratio between the 0wk and 1wk time points. However, it was shown with statistical significance that both the static and perfusion systems showed a significant decrease in redox ratios from the 1 to 2wk time points. The drop in redox ratio was larger for the static culture, but significant at $p<0.05$ nonetheless ($p<0.001$ for perfusion). It was also observed through a two sample t-test for comparing means that the mean redox ratios for static and perfusion cultures at each time point were significantly different from one another for at least $p<0.01$ at each time point. Considering that these tissues were grown following identical protocols and were both held in identical mediums, the difference in redox ratio values for each of them can only be attributed to the different bioreactor environments they were cultured in (static vs.

perfusion). It would appear the perfusion makes it slightly more difficult for the tissue to become metabolically active immediately (perhaps some cells were washed away during perfusion).

It is speculated by Quinn et al., 2011, that this decrease in redox ratio is a result of adipogenesis beginning, which eventually lets off at about day 57 when the scaffold can't handle any more lipid accumulation. Through this experiment, it has been shown with statistical significance that a decrease in redox ratio, and therefore increase in metabolic activity does occur between weeks one and two. As mentioned before when discussing the effects of drugs on adipose tissue, lipogenesis is a cause for metabolic activity when it occurs (anabolism).

Histology

To complement the redox maps and data acquired from the noninvasive imaging analyses, histological H&E stained images were taken as well to gain an understanding of cellular proliferation, cellular localization, and ECM growth within the tissues. Images of the H&E stained samples taken at the edge and the middle sections of the tissues are shown in Figures 22 and 23 respectively. The tissue 'edges' as they are described are again the bottom surfaces of the tissues that are to be imaged through redox ratio analysis. The 'middle' images are from the same circular cross sectional area of the perfusion inflow and outflow ports of the bioreactor chambers taken from halfway within the tissue.

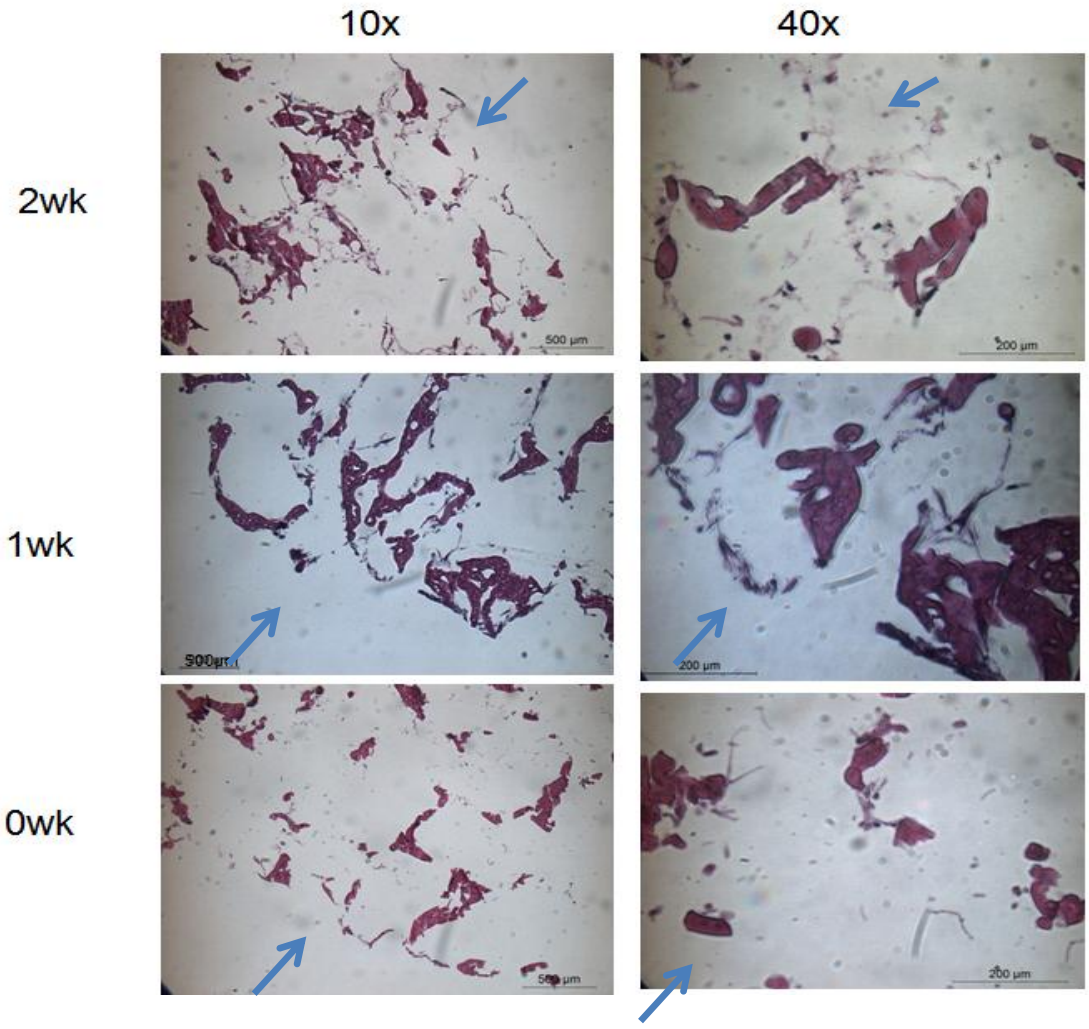

Figure 22. H&E stained images taken of the edges of the adipose samples after 0, 1, and 2wks in perfusion. Images were acquired at 10x and 40x. Like in the previously described static cultures, the dark purple structures are the silk scaffold, the lighter purple is ECM, and the dark spots within elongated structures are nuclei within cells. The blue arrows specify the location of the edges of the tissues.

As observed in Figures 22 and 23, there is very little, if any, ECM present in the 0wk samples. This is most likely because those samples were just seeded with adipocytes two days prior, which is not sufficient to allow for any considerable ECM growth. There is however some ECM present in the 1 and 2wk cultures. This is most likely a result of increased cellularity within the tissue and added time for the cells to build an extracellular matrix. It should be mentioned that the ECM of adipose tissue primarily consists of a

loose collagenous matrix whose sole purpose is to hold the adipocytes together and prevent the adipose tissue from becoming a completely viscous material (maintains some elasticity). Given the observations made earlier in the static culture, it would be expected that if these tissues had remained in culture for longer times, that the cellularity of the tissues would have only increased while a more robust and expansive ECM developed.

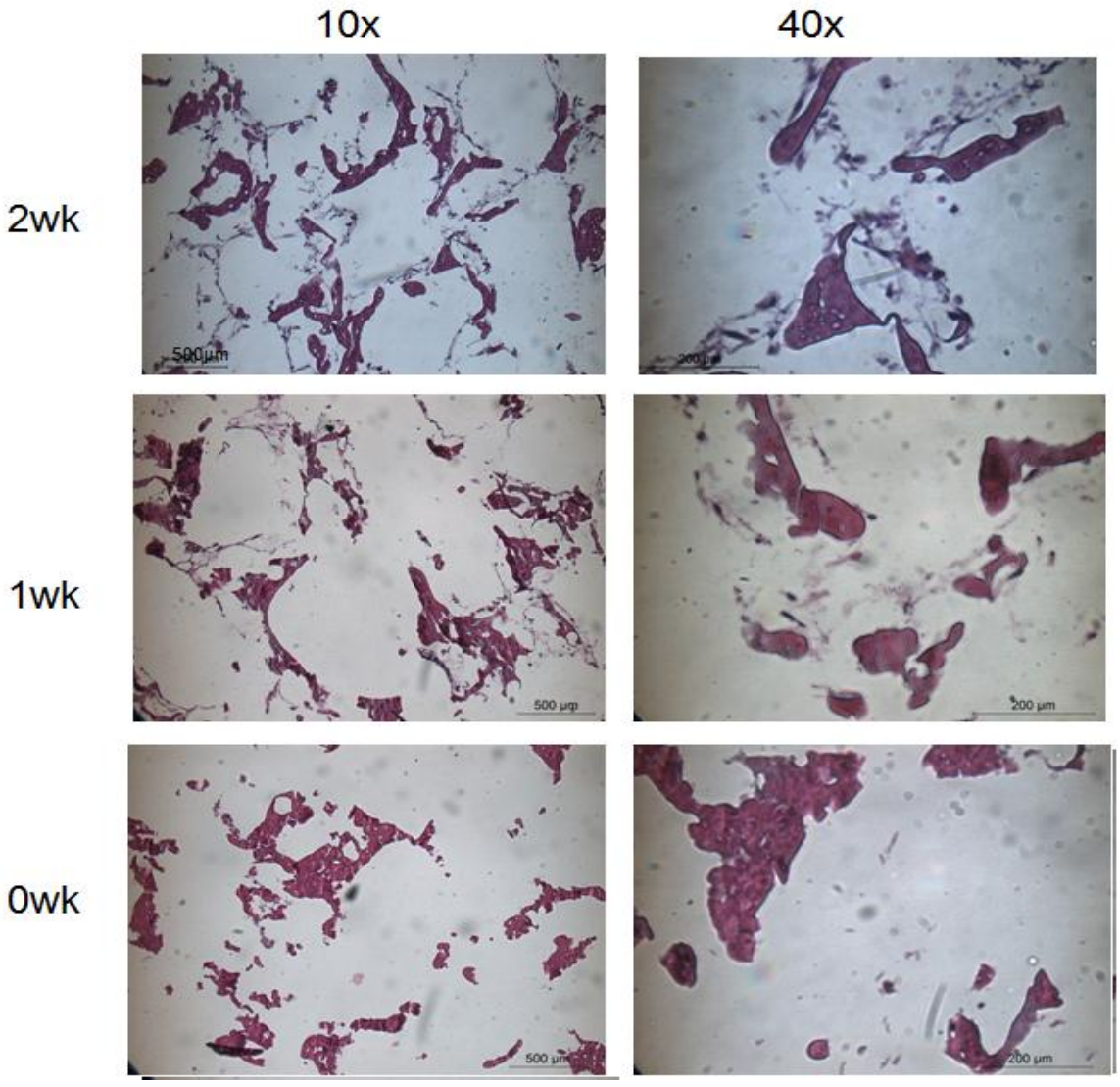

Figure 23. H&E stained images taken of the middle section of adipose samples after 0, 1, and 2wks in perfusion. Images were acquired at 10x and 40x.

FUTURE WORK

Given the capabilities of bioreactor system proposed here for long term continued perfusion flow in a sterile environment with a cover glass imaging interface and media extraction capabilities, the system can be used for a variety of future experiments and research paths.

ELONGATED TIMESCALE

The experiment outlined above was conducted on a three week timeline to emulate the work done by Kang, et al. However, the performance of the bioreactor system throughout the test, and the state of the samples that were imaged after two weeks perfusion suggest that the system is more than capable of longer perfusion times to accommodate longer experiments. This affords the opportunity to emulate the work done by Quinn, et al where redox ratio and histological information was gathered on adipose tissue in static culture for a span of up to six months. This data provides a means of comparison to understand how a perfusion environment affects the maturity path of the engineered 3D human adipose tissues proposed by Kang, et al relative to those grown in static culture. Key parameters for comparison would be how redox ratios change over time and the presence and growth rate of lipids within the tissues as a function of Oil Red O staining.

DRUG DELIVERY/DISEASE MODEL

As described in the Background section, there are a variety of FDA-approved drugs and biomolecules whose effects on adipose tissue have been well documented. Many of these affects have a direct correlation to metrics that can be observed through the imaging protocols described before (i.e., Rosiglitazone causing a decrease in cell size and increase in lipolysis/lipogenesis accompanied by an increase in metabolic activity, so decreased redox ratio (Kahn et al., 2005; Mcternan et al., 2002). Media extraction abilities also afford the opportunity for protein and other biomolecule detection throughout drug testing. Anti-diabetics, including Thiazolidinediones, Sulfonylureas, and Meglitinides can be used – previous work shows adipose responding to TZDs with decreased leptin expression, increased LPL and HSL protein expression, and a net lipid gain (Kahn et al., 2000; Mcternan et al., 2002). Obesity is associated with inflammation in adipose tissue caused by macrophage infiltration, so TNF-α inhibitors (Methotrexate) have been studied and shown to decrease leptin secretion and increase adiponectin in excised adipose tissue (Gambero et a.,. 2011). Excess Insulin and Norepinephrine has shown increased glycerol release (sign of increased lipolysis, or net lipid loss) in *in vitro* adipocyte cultures (Mcternan et al., 2002).

Anti-diabetics, including Thiazolidinediones, Sulfonylureas, and Meglitinides can be used – LPL and HSL expression measured through western/northern blot analysis, FFA and glycerol assays. Immunohistochemistry for detection of CD-31 and HIF-1α. Oil Red O staining for lipid droplets. H&E staining shows general cell density, localization, and ECM growth. Adipocyte inflammation/obesity measured through inflammatory markers,

i.e. TNF-α via biochemical assays. Also correlated with lipid droplet size and leptin secretion.

FULL TISSUE IMAGING

One of the more severe limitations of the system described here is the poor penetration depth afforded by the imaging methods described (200 µm). The reason for this poor penetration depth is the limitations of the 63x objective used. The reason a water-immersed 63x objective is used is for the higher magnification levels it provides in order to achieve a high resolution of the cells and ECM/scaffold structure within the three 40 µm image stack depths. This leads to the conclusion that in order to be able to penetrate deeper into the tissue, some image resolution will be sacrificed (resolution to penetration depth relationship shown below in Figure 24).

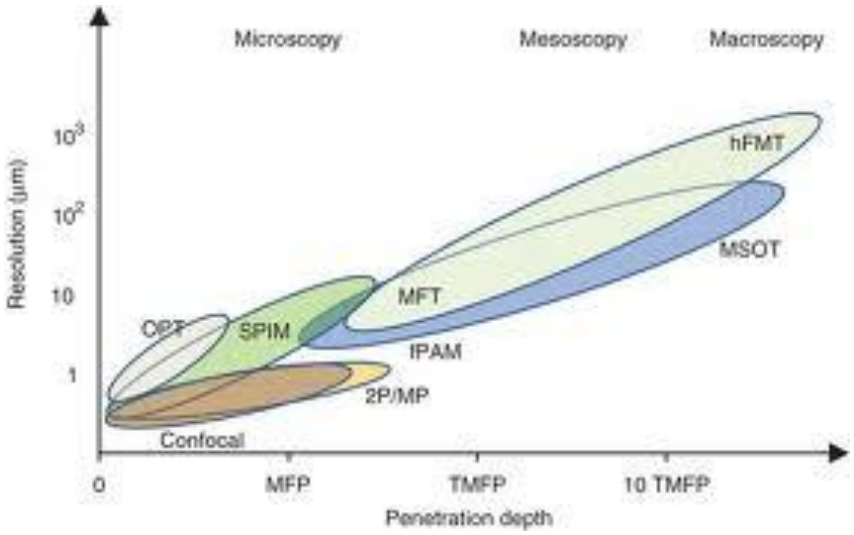

Figure 24. Regardless of imaging modality, there is a significant correlation between the loss in resolution of an imaging method and the penetration depth of the imaging technique (Ntziachristos et al., 2010)

The confocal system available during this research has a 10x, 20x, and 63x objective with tissue penetration depths through a No. 1.5 thickness cover glass of 11mm, 0.57mm, and 0.22mm respectively. By imaging the adipose tissue samples from within the bioreactor chamber (custom or 3DKUBE™) using either the 10x or 20x objectives, the penetration depth allowed can be significantly improved.

If a 10x objective were used for the purpose of imaging throughout the entirety of the tissue sample, resolution would definitely be lost. This causes a major setback in the ability to isolate the fluorescent contributions of both NAD(P)H and FAD when performing redox ratio analysis. However, it was shown in both this work and previously performed static work (Quinn et al., 2011) that the redox ratio of the cells does not significantly decrease as a function of depth. If a 10x (or even 20x) objective were to be used for higher penetration depths, the most important data that could be acquired from the imaging would be the differences in cellularity as a function of depth (which has been demonstrated to be significant). If the ability to perform redox ratio analysis was lost but it could be shown that the redox ratio was unlikely to change as a function of depth, then the improved analysis offered by a 10x objective to determine the cellularity of deeper sections of the tissue would be considered useful. This would be especially significant in comparing the differences in cellularity as a function of tissue depth between static and perfusion culture which has been demonstrated in other work to be significant (Grayson et al., 2010).

The difficulty of this future plan lies in re-writing the MatLab algorithm to accurately identify and classify different objects in the 10x images as cells and silk. If a similar linear discriminant analysis can be performed at a lower magnification level to differentiate between the different structures within the images acquired using a 10x objective then a count of the cells can be performed to determine cellularity. This task may be alleviated by increasing the bit resolution of each pixel acquired in each image, and targeting multiple fluorophores (collagen, lipofuscin, NAD(P)H, FAD, and silk) and use a more macro-scale analysis of the fluorescent intensities gathered at different combinations of ex/em wavelengths to determine key differences between samples exhibiting high levels of cell proliferation with tissue growth and samples that may just be unseeded silk scaffolds.

CONCLUSION

The system proposed in this research is for a perfusion bioreactor system compatible with advanced imaging capabilities under high magnification levels that can sustain continuous flow in a sterile environment over weeks to months with media replenishment and extraction capabilities. The aim of this system was to show that a more physiologically relevant system could be built that could accommodate a metabolic/biochemical and morphological analysis of a particular engineered 3D human tissue. The purpose of this aim is to improve the methods by which human tissues are studied for the purposes of disease models, drug screening, developmental biology, and others.

The perfusion bioreactor system built did show the ability to sustain a sterile culture over the span of weeks, and demonstrated potential to go on for months. The chambers were compatible with the mechanics of the imaging analysis required to perform redox ratio analysis on the tissue samples *in situ.*

The purpose of the perfusion element of the system was to provide a more physiologically relevant environment for the tissues to mature in when compared to the usual static culture. The project was chosen with a particular tissue/tissue engineering protocol combination so that there would be a complimentary static analysis of adipose tissue available for comparison with the perfusion data acquired here. Both the static and perfusion environments should similar trends with regards to the redox ratios remaining stagnant for the first week of testing, but then dropping off slightly after two weeks. This data was confirmed as significant to the $p<0.05$ level for both static and perfusion cultures through a two sample t-test for comparing means.

WORKS CITED

Albracht, Simon PJ. "The Reaction of NADPH with Bovine Mitochondrial NADH: Ubiquinone Oxidoreductase Revisited." *J Bioenerg Biomembr* 42 (2010): 279-92. Print.

Boden, G., C. Homko, M. Mozzoli, L. C. Showe, C. Nichols, and P. Cheung. "Thiazolidinediones Upregulate Fatty Acid Uptake and Oxidation in Adipose Tissue of Diabetic Patients." Diabetes 54.3 (2005): 880-85. Print.

Boucher JR, R. C., P. A. Bromberg, and J. T. Gatzy. "Airway Transepithelial Electric Potential in Vivo: Species and Regional Differences." Jan. 1980. Web. <http://www.ncbi.nlm.nih.gov/pubmed/6101591>.

Breunig, Hans Georg, Hauke Studier, and Karsten König. "Multiphoton Excitation Characteristics of Cellular Fluorophores of Human Skin in Vivo." *Optics Express* 18.8 (2010): 7857. Print.

Chao, Lily, Bernice Marcus-Samuels, Mark M. Mason, Jaideep Moitra, Charles Vinson, Elif Arioglu, Oksana Gavrilova, and Marc L. Reitman. "Adipose Tissue Is Required for the Antidiabetic, but Not for the Hypolipidemic, Effect of Thiazolidinediones." Journal of Clinical Investigation 106.10 (2000): 1221-228. Print.

CONGRESSIONAL BUDGET OFFICE "Director's Blog » Blog Archive » Pharmaceutical R&D and the Evolving Market for Prescription Drugs." Director's Blog. Web. 01 Dec. 2010. <http://cboblog.cbo.gov/?p=399>.

Conklin, Matthew W., Paolo P. Provenzano, Kevin W. Elicieiri, Ruth Sullivan, and Patricia J. Keely. "Fluorescence Lifetime Imaging of Endogenous Fluorophores in Histopathology Sections Reveals Differences Between Normal and Tumor Epithelium in Carcinoma In Situ of the Breast." *Cell Biochem Biophys* 53 (2009): 145-147. Print.

Dicker, D., P. Herskovits, M. Katz, E. Atar, and G. N. Batar. "Computed Tomography Study of the Effect of Orlistat on Visceral Adipose Tissue Volume in Obese Subjects." Web. 01 Dec. 2010. <http://www.ncbi.nlm.nih.gov/pubmed/20803876>.

Dunham, S. "Lessons from the Cat: Development of Vaccines against Lentiviruses." Veterinary Immunology and Immunopathology 112.1-2 (2006): 67-77. Print.

"Economic Costs of Diabetes in the U.S. in 2002." Diabetes Care 26.3 (2003): 917-32. Print.

Fujii, Satoshi, and Tetsuhiko Yoshimura. "Detection and Imaging of Endogenously Produced Nitric Oxide with Electron Paramagnetic Resonance Spectroscopy." *Antioxidants & Redox Signaling* 2.4 (2000): 879-901. Print.

Gambero, A., de Oliveira C,. Acedo S. C., Rocha, T., “Effects of Methotrexate in the Inflammatory Alterations Associated to Obesity: an In vivo and In vitro study,” *Pharmacological Research*, vol. 9, pp. 341-346, 2006

Ghukasyan, Vladimir, Tatyana Buryakina, and Fu-Jen Kao. "Metabolic Mapping of Cell Culture Growth by NADH Fluorescence Lifetime Imaging." *Multiphoton Microscopy in the Biomedical Sciences* 7183 (2009). Print.

Georgakoudi, Irene, William L. Rice, Marie Hronik-Tupaj, and David L. Kaplan. "Optical Spectroscopy and Imaging for the Noninvasive Evaluation of Engineered Tissues." *Tissue Engineering Part B: Reviews* 14.4 (2008): 321-40. Print.

Grayson, Warren L., Mirjam Fröhlich, Darja Marolt, Jeffrey M. Gimble, Nevenka Kregar-Velikonja, and Gordana Vunjak-Novakovic. "Bone Grafts Engineered from Human Adipose-Derived Stem Cells in Perfusion Bioreactor Culture." *Tissue Engineering Part A* 16.1 (2010): 179-89. Print.

Grayson, Warrem L., Darja Marold, Sarindr Bhumirantana, Mirjam Frohlich, Edward X. Guo, and Gordana Vunjak-Novakovic. "Optimizing the Medium Perfusion Rate in Bone Tissue Engineering Bioreactors." *Biotechnology and Bioengineering* 108.5 (May 2011): 1159-170. Print.

Hanson, Graeme, Lawrence J. . Berliner, John H. Enemark, A. V. Astashkin, and A. M. Raitsimring. *Metals in Biology Applications of High-resolution EPR to Metalloenzymes*. Vol. 29. New York: Springer, 2010. 121-69. Print.

"In Vitro and Alternative Assay Services." 26 Nov. 2006. Web. <http://www.mbresearch.com/invitro.htm>.

Job, C. K. "Nine-banded Armadillo and Leprosy Research." Indian Journal of Pathology and Microbiology 46.4 (2003): 541-50. Web.

Kadantsev, Eugene S., and Tom Ziegler. "First-principles Calculation of Parameters of Electron Paramagnetic Resonance Spectroscopy in Solids." *Magnetic Resonance in Chemistry* 48.S1 (2010): S2-S10. Print.

Kahn, C. Ronald, Lihong Chen, and Shmuel E. Cohen. "Unraveling the Mechanism of Action of Thiazolidinediones." *Journal of Clinical Investigation* 106.11 (2000): 1305-307. Print.

Kang, Jennifer H., Jeffrey M. Gimble, and David L. Kaplan. "13. In Vitro 3D Model for Human Vascularized Adipose Tissue." 15 Aug. 2009. Web. <http://www.ncbi.nlm.nih.gov/pmc/articles/PMC2792112/>.

Kirkpatrick, Nathaniel D., Changping Zou, Molly A. Brewer, William R. Brands, Rebekah A. Drezek, and Urs Utzinger. "Endogenous Fluorescence Spectroscopy of Cell Suspensions for Chemopreventive Drug Monitoring." Photochemistry and Photobiology (2004). Print.

Kluge, Jonathan A., Gary G. Leisk, Robyn D. Cardwell, Alexander P. Fernandes, Michael House, Andrew Ward, Luis Dorfmann, and David L. Kaplan. "Bioreactor System Using Noninvasive Imaging and Mechanical Stretch for Biomaterial Screening." *Annals of Biomedical Engineering* 39.5 (May 2011): 1390-402. Print.

Koenig, Karsten, and Iris Riemann. "High-resolution Multiphoton Tomography of Human Skin with Subcellular Spatial Resolution and Picosecond Time Resolution." *Journal of Biomedical Optics* 8.3 (2003): 432. Print.

Kola, Ismail, and Landis, John "Access : Can the Pharmaceutical Industry Reduce Attrition Rates? : Nature Reviews Drug Discovery." Nature Publishing Group : Science Journals, Jobs, and Information. Web. 01 Dec. 2010. <http://www.nature.com/nrd/journal/v3/n8/full/nrd1470.html>.

Kumar, Naveen, Subheet Jain, Anshu Gupta, and Ashok Kumar Tiwary. "Spermicidal Activity of Sulfonylureas and Meglitinide Analogues: Role of Intrasperm Ca2+ Elevation." *Journal of Pharmacy and Pharmacology* 60.3 (2008): 323-30. Print.

Lee, Jyh-Hong, Szu-Yu Chen, Che-Hang Yu, Shih-Wei Chu, Li-Fang Wang, Chi-Kuang Sun, and Bor-Luen Chiang. "Noninvasive in Vitro and in Vivo Assessment of Epidermal Hyperkeratosis and Dermal Fibrosis in Atopic Dermatitis." *Journal of Biomedical Optics* 14.1 (2009): 014008. Print.

Leloup, Corinne, Louis Casteilla, Audrey Carrière, Anne Galinier, Alexandre Benani, Lionel Carneiro, and Luc Pénicaud. "Balancing Mitochondrial Redox Signaling: A Key Point in Metabolic Regulation." *Antioxidants & Redox Signaling* (2010): 101026130651058. Print.

Lenz, Eva M. "Nuclear Magnetic Resonance (NMR)-Based Drug Metabolite Profiling." *Metabolic Profiling, Methods in Molecular Biology* (2011): 299-319. Print.

Lleres, David, Samuel Swift, and Angus Lamond. "Detecting Protein-Protein Interactions In Vivo with FRET Using Multiphoton Fluorescence Lifetime Imaging Microscopy (FLIM)." *Current Protocols in Cytometry* (October 2007): 12.10.1-2.10.19. Print.

Lombardi-Borgia, S., P. Schlupp, W. Mehnert, and M. Schafer-Korting. "In Vitro Skin Absorption and Drug Release – A Comparison." ScienceDirect. 2007. Web.

Maidhof, Robert, Anna Marsano, Eun Jung Lee, and Gordana Vunjak-Novakovic. "Perfusion Seeding of Channeled Elastomeric Scaffolds with Myocytes and Endothelial Cells for Cardiac Tissue Engineering." *Biotechnology Progress* (2010): NA. Print.

McCully, K. "Nuclear Magnetic Resonance Spectroscopy: Its Role in Providing Valuable Insight Into Diverse Clinical Problems." *Chest* 116.5 (1999): 1434-441. Print.

McTernan, P. G., A. L. Harte, L. A. Anderson, A. Green, S. A. Smith, J. C. Holder, A. H. Barnett, M. C. Eggo, and S. Kumar. "Insulin and Rosiglitazone Regulation of Lipolysis and Lipogenesis in Human Adipose Tissue In Vitro." Diabetes 51.5 (2002): 1493-498. Print.

Netzlaff, F., C. M. Lehr, and U. F. Schaefer. "The Human Epidermis Models Episkin, SkinEthic and EpiDerm : An Evaluation of Morphology and Their Suitability for Testing Phototoxicity, Irritancy, Corrosivity, and Substance Transpor." July 2005. Web. <http://www.ncbi.nlm.nih.gov/pubmed/15913972>.

Noctor, Graham. "Metabolic Signalling in Defence and Stress: the Central Roles of Soluble Redox Couples." *Plant, Cell and Environment* 29.3 (2006): 409-25. Print.

Ntziachristos, Vasilis. "Going Deeper than Microscopy: the Optical Imaging Frontier in Biology." *Nature Methods* 7.8 (2010): 603-14. Print.

Oakes, N. D., P. G. Thalen, S. M. Jacinto, and B. Ljung. "Thiazolidinediones Increase Plasma-Adipose Tissue FFA Exchange Capacity and Enhance Insulin-Mediated Control of Systemic FFA Availability." Diabetes 50.5 (2001): 1158-165. Print.

Olefsky, Jerrold M. "Treatment of Insulin Resistance with Peroxisome Proliferator–activated Receptor γ Agonists." Journal of Clinical Investigation 106.4 (2000): 467-72. Print.

Ostrander, J. H., C. M. McMahon, S. Lem, S. R. Millon, J. Q. Brown, V. L. Seewaldt, and N. Ramanujam. "Optical Redox Ratio Differentiates Breast Cancer Cell Lines Based on Estrogen Receptor Status." Cancer Research 70.11 (2010): 4759-766. Print.

Paaske. "VASCULAR PERMEABILITY IN ADIPOSE TISSUE MEASURED BY THE SINGLE INJECTION EXTERNAL REGISTRATION METHOD." Acta Physiologica Scaninavica Supplementum 396 (1973). Print.

Paul, Steven M., Daniel S. Mytelka, Charles C. Persinger, Bernard H. Munos, Stacy R. Lindborg, Christopher T. Dunwiddie, and Aaron L. Schacht. "How to Improve R&D Productivity: the Pharmaceutical Industry's Grand Challenge." Nature Reviews Drug Discovery (9). Print. March 2010

Pavet, V. "Ascorbic Acid Deficiency Activates Cell Death and Disease Resistance Responses in Arabidopsis." Plant Physiology 139.3 (2005): 1291-303. Print.

Poumay, Yves, and Alain Couquette. "Modelling the Human Epidermis in Vitro: Tools for Basic and Applied Research." 29 Sept. 2006. Web. <http://www.ncbi.nlm.nih.gov/pmc/articles/PMC1705521/>.

Provenzano, Paolo P., Curtis T. Rueden, Steve M. Trier, Long Yan, Suzanne M. Ponik, David R. Inman, Patricia J. Keely, and Kevin W. Eliceiri. "Nonlinear Optical Imaging and Spectral-lifetime Computational Analysis of Endogenous and Exogenous Fluorophores in Breast Cancer." Journal of Biomedical Optics 13.3 (2008): 031220. Print.

Quisth, V., S. Enoksson, E. Blaak, E. Hagström-Toft, P. Arner, and J. Bolinder. "Major Differences in Noradrenaline Action on Lipolysis and Blood Flow Rates in Skeletal Muscle and Adipose Tissue in Vivo." Diabetologia 48.5 (2005): 946-53. Print.

Rhee, S. G. "Redox Signaling: Hydrogen Peroxide as Intracellular Messenger." Experimental and Molecular Medicine 2nd ser. 31 (June 1999): 53-59. Print.

Rice, William L., David L. Kaplan, and Irene Georgakoudi. "Quantitative Biomarkers of Stem Cell Differentiation Based on Intrinsic Two-photon Excited Fluorescence." JBO Letters. 18 Dec. 2007. Web.

Rice, William L., David L. Kaplan, and Irene Georgakoudi. "Two-Photon Microscopy for Non-Invasive Quantitative Monitoring of Stem Cell Differentiation." 2010. Web. <http://www.plosone.org/article/info:doi/10.1371/journal.pone.0010075>.

Roberts, Michael S., Yuri Dancik, Tarl W. Prow, Camilla A. Thorling, Lynlee L. Lin, Jeffrey E. Grice, Thomas A. Robertson, Karsten König, and Wolfgang Becker. "Non-invasive Imaging of Skin Physiology and Percutaneous Penetration Using Fluorescence Spectral and Lifetime Imaging with Multiphoton and Confocal Microscopy." European Journal of Pharmaceutics and Biopharmaceutics 77.3 (2011): 469-88. Print.

Skala, Melissa, and Nirmala Ramanujam. "Multiphoton Redox Ratio Imaging for Metabolic Monitoring In Vivo." Advanced Protocols in Oxidative Stress II. Vol. 594. Humana, a Part of Springer Science+Business Media,LLC, 2010. 155-62. Print.

Skoog, Douglas A., F. James. Holler, and Stanley R. Crouch. Principles of Instrumental Analysis. Belmont, CA: Thomson Brooks/Cole, 2007. Print.

Spasojević, Ivan. "Free Radicals and Antioxidants at a Glance Using EPR Spectroscopy." Critical Reviews in Clinical Laboratory Sciences 48.3 (2011): 114-42. Print.

Spasojevic, Ivan, Milos Mojovic, Aleksandar Ignjatovic, and Goran Bacic. "The Role of EPR Spectroscopy in Studies of the Oxidative Status of Biological Systems and the Antioxidative Properties of Various Compounds." Journal of Serbian Chemical Society 76.5 (2011): 647-77. Print.

Tingle, M. D., and N. A. Helsby. "Can in Vitro Drug Metabolism Studies with Human Tissue Replace in Vivo Animal Studies?" 2 Aug. 2005. Web. <http://www.sciencedirect.com/science?_ob=ArticleURL&_udi=B6T6D-4GSJXJW2&_user=201547&_coverDate=02%2F28%2F2006&_rdoc=1&_fmt=high&_orig=search&_origin=search&_sort=d&_docanchor=&view=c&_acct=C000014058&_version=1&_urlVersion=0&_userid=201547&md5=7032c44f2bb35dd22973929cdca85239&searchtype=a>.

Vanea, Emilia, Nicolas Charlier, Julie DeWever, Mustapha Dinguizli, Olivier Feron, Jean-François Baurain, and Bernard Gallez. "Molecular Electron Paramagnetic Resonance Imaging of Melanin in Melanomas: a Proof-of-concept." NMR in Biomedicine 21.3 (2008): 296-300. Print.

White/Kiyatec. "Three-Dimensional (3D) Cell Culture In Situ Histological Embedding." Www.kiyatec.com. Kiyatec, Inc. Pendelton, SC 29670, 2011. Web.

Wilcox, Dean E., and Roger P. Smith. "Detection and Quantification of Nitric Oxide Using Electron Magnetic Resonance Spectroscopy." Methods: A Companion to Methods in Enzymology (1995): 59-70. Print.

Yu, Fa-Xing, Ru-Ping Dai, Shuang-Ru Goh, Lei Zheng, and Yan Luo. "Logic of a Mammalian Metabolic Cycle." Landes Bioscience 8.5 (March 2009): 773-79. Print.

Zghoul, N., Fuchs, R., Lehr, C.M., Schaefer "RECONSTRUCTED SKIN EQUIVALENTS FOR ASSESSING PERCUTANEOUS DRUG ABSORPTION FROM PHARMACEUTICAL FORMULATIONS." MatTek in Vitro 3-D Human

TISSUE Equivalents - Non-Animal Alternative Test. Web. 01 Dec. 2010. <http://www.mattek.com/pages/abstracts/221>.

Zhuo, Ying, Ruo Yuan, Yaqin Chai, Zhongju Song, Wen Jiang, Huilan Su, Xin Che, and Jingjing Li. "Depth-cumulated Epithelial Redox Ratio and Stromal Collagen Quantity as Quantitative Intrinsic Indicators for Differentiating Normal, Inflammatory, and Dysplastic Epithelial Tissues." Chemical Communications 46.36 (2010): 6750-752. Print.

APPENDIX A: BIOREACTOR MACHINE DRAWINGS

APPENDIX B: BIOREACTOR COMPONENTS

Silicon (platinum cured) tubing, (1/16”)IDx25ft, Cole-Parmer, EW-95802-02

$25.25

Polypropylene Barbed Female Luerx(1/16”)hose barb, Cole-Parmer, EW-45500-00

$7.55

Polypropylene Barbed Male Luer w/lock ring x(1/16”) hose barb, Cole-Parmer, EW-45503-00

$8.25

Straight Through Tube Fitting with Classic Series Barbs, 1/16" (1.6 mm) ID Tubing, Clear Polycarbonate 100pk, ValuePlastics, AA-9

$25.10

3DKUBE™ Independent Chambers, Kiyatec, 3D020

$220.00

VWR® Black Rubber Stoppers, Solid, Size 3, 1Pack, VWR, 59580-149

$44.93

Masterflex PharMed BPT Tubing, L/S #13, 25’, Cole-Parmer, SI-06508-13

$69.00

Circular Cover Glass, 1.5 Thickness, 12mm diameter, Fisher Scientific, 12-545-81

$183.76

Loctite 4541, McMaster-Carr, 1818A491

$25.24

L/S Modular Digital Dispensing Drives - L/S® Modular brushless digital dispensing drive, 10 to 600 rpm, 115/230 VAC, Cole-Parmer, EW-77301-20

$2,175.00